Time evolution of proton magnetization in the spin-rotating frame of an ensemble of interacting pairs of methyl groups: A study of the magnetic-flux effect

J. Peternelj
Institute J. Stefan, University of Ljubljana, Ljubljana, Slovenia

A. Damyanovich and M. M. Pintar
Department of Physics, University of Waterloo, Waterloo, Ontario, Canada N2L 3G1
(Received 3 September 1993)

The effect of an external magnetic field on a pair of interacting methyl groups in a solid lattice is considered. Because of the consequent appearance of a gauge potential in the total Hamiltonian of the system, its time-reversal invariance is broken, leading to the splitting of otherwise degenerate E levels. Since transitions between these states influence the time evolution of the Zeeman polarization in the rotating frame, calculations are presented from which the spectra for a particular energy-level scheme are obtained in the case of a fictitious crystal and a polycrystalline sample. It is shown that the appearance of spectral features at frequencies other than integer multiples of the rf frequency ω_1 can be taken as evidence of transitions between magnetic-flux-split E states. The polycrystalline spectrum is compared to the experimental spectrum of two solids with qualitative agreement if the effective charge on the protons is 0.15 and 0.10, respectively, of the elementary charge.

I. INTRODUCTION

Studies of the dynamics of molecular systems in a magnetic field have shown that the Born-Oppenheimer approximation leads to a value of the effective charge q, equal to the bare nuclear charge.[1] This value of q (which is a measure of the strength of the coupling between the nuclear spins and the external field) does not, however, take into account the effects of electronic screening experienced by each nucleus, the magnitude of which is not yet accurately known.

Consider a "rigid" methyl group undergoing tunneling motion around its symmetry axis in an external magnetic field $\mathbf{H}_0$. Since in a nonrelativistic approximation the spatial and spin degrees of freedom are not coupled, we may write the Hamiltonian as[2]

$$H=H_e+\frac{\hbar^2}{2I}\left[-\frac{i\partial}{\partial\gamma}-\frac{3e}{hc}\Phi-L_\zeta\right]^2+V_3(\gamma)\ , \quad (1.1)$$

where H_e is the electronic Hamiltonian,

$$H_e=-\frac{\hbar^2}{2m}\sum_i\nabla_i^2+U+\mu_B\mathbf{H}_0\cdot\mathbf{L}+\frac{e^2}{8m^2c^2}\mathbf{H}_0\cdot I_e\cdot\mathbf{H}_0\ . \quad (1.2)$$

In (1.2), m and $-e$ are the electronic mass and charge, respectively, $-i\hbar\nabla_i\equiv\mathbf{p}_i$ is the momentum operator of the ith electron, $\hbar\mathbf{L}\equiv\sum_i\mathbf{r}_i\times\mathbf{p}_i$ is the total orbital angular momentum of the electrons, and I_e is the tensor of inertia of electrons. All these operators are defined with respect to the coordinate system (ξ,η,ζ) fixed to the methyl group, with the ζ axis parallel to the methyl symmetry axis. (For the time being, the direct coupling of the spins among themselves and with $\mathbf{H}_0$ is omitted.) In addition, I is the moment of inertia of the methyl group rotating around its symmetry axis, γ is the angle of rotation, and Φ represents the magnetic flux through the circular loop traced out by the protons, equal to

$$\frac{3e}{2\pi c}\Phi=\boldsymbol{\varepsilon}_3\cdot I\boldsymbol{\Omega}\ , \quad (1.3)$$

where $\boldsymbol{\varepsilon}_3$ is a unit vector along the symmetry axis. $\boldsymbol{\Omega}=e\mathbf{H}_0/2m_pc$ is the Larmor frequency of the protons in the field $\mathbf{H}_0$, m_p is the proton mass, and $\mu_B=e\hbar/2mc$ is the Bohr magneton. Finally, the potential energies U and V_3 are the Coulomb interactions of all charged particles in the methyl group and its hindering potential, respectively.

The solution of the eigenvalue equation

$$H\Psi=E\Psi \quad (1.4)$$

is sought in the form

$$\Psi(\gamma,\mathbf{r}_i)=\sum_n\psi_n(\gamma)\varphi_n(\gamma;\mathbf{r}_i)\ , \quad (1.5)$$

where $\mathbf{r}_i$ is an abbreviation for the complete set $\mathbf{r}_1,\mathbf{r}_2,\ldots,\mathbf{r}_i$. The electronic wave functions $\varphi_n(\gamma;\mathbf{r}_i)$ are the orthonormalized solutions of

$$H_e\varphi_n(\gamma;\mathbf{r}_i)=U_n(\gamma)\varphi_n(\gamma;\mathbf{r}_i)\ . \quad (1.6)$$

The eigenfunction (1.5) is not determined until the boundary condition is specified. We choose $\Psi(\gamma,\mathbf{r}_i)$ to be single valued with respect to γ, i.e.,

$$\Psi(\gamma+2\pi,\mathbf{r}_i)=\Psi(\gamma,\mathbf{r}_i)\ , \quad (1.7)$$

which does not imply, however, that $\psi_n(\gamma)$ and $\varphi_n(\gamma;\mathbf{r}_i)$, considered separately, ought to be single valued. Our choice of (1.7) is based on the observation made by

Merzbacher[3] that the representation of a rotating molecule by a rigid body is an idealization. In reality, the configuration space of the particles forming the molecule is simply connected, and consequently (1.7) holds.

The temperature range of interest to us is such that the methyl group is in the ground electronic state φ_0. Moreover, the energy difference between the electronic ground and first excited state is of the order[4] of 10 eV, while the energy scale of the rotational motion is determined by the rotational constant $\hbar^2/2I \doteq 0.65$ meV. Therefore, for the purposes of studying the tunneling motion, we may write (1.5) as

$$\Psi(\gamma,\mathbf{r}_i)=\psi(\gamma)\varphi_0(\gamma;\mathbf{r}_i) . \tag{1.8}$$

In addition, $\mu_B \doteq 5.7\times10^{-5}$ eV/T and $e^2I_e/8m^2c^2 \doteq 10^{-10}$ eV/T^2, so that when dealing with magnetic fields of the order of 1 T, we may treat the third term in (1.2) as a small perturbation, discarding the fourth term altogether. Finally, it can be shown[2] that $\psi(\gamma)$ obeys

$$\left\{\frac{\hbar^2}{2I}\left[-\frac{id}{d\gamma}-\frac{3q}{hc}\Phi\right]^2+V_3(\gamma)-E\right\}\psi(\gamma)=0 , \tag{1.9}$$

where q is the effective charge given by

$$q>e\left[1-4\frac{(m_p/m)\hbar/2I}{U_1^{(0)}-U_0^{(0)}}\langle\varphi_0^{(0)}|L_\xi^2|\varphi_0^{(0)}\rangle\right] . \tag{1.10}$$

Here $(m_p/m)\hbar^2/2I_0 \doteq 1.19$ eV and $\varphi_0^{(0)}$ is the ground electronic state in the absence of the magnetic field $\mathbf{H}_0$, while $U_0^{(0)}$ and $U_1^{(0)}$ are the ground and first excited electronic energies.

The methyl groups encountered in molecular crystals are always covalently bonded to the molecule on which they reside, and thus all four bonding orbitals of the carbon atom are doubly occupied. Therefore it seems reasonable to assume that the ground electronic state closely resembles that of an isolated CH_4 molecule. Consequently, $\varphi_0^{(0)}$ is taken to be an $^1A_1$ singlet where A_1 is the completely symmetrical one-dimensional representation of the point group C_{3v}. We require, moreover, that

$$\psi(\gamma+2\pi)=\psi(\gamma) , \tag{1.11}$$

in accordance with (1.7). Estimating $U_1^{(0)}-U_0^{(0)} \cong 22$ eV and using the expressions for the bonding orbitals of methane,[5] we obtain[2] $q>0.24e$.

It is at this point worth mentioning the view advocated by Clough, McDonald, and Zelaya.[6] These authors suggest that the proper description of methyl rotational motion in a nonstationary crystal lattice should employ, in the low-temperature limit, multivalued wave functions instead of the single-valued ones as required by (1.11). However, a description of methyl-group dynamics based on the use of multivalued wave functions is unitarily equivalent to the description based on (1.11) if an extra gauge term is added to (1.9). This ambiguity in the choice of boundary conditions is a general property of the Hamiltonian (1.9), which, because it is not essentially self-adjoint,[7] admits a one-parameter family of self-adjoint extensions:

$$\psi(\gamma+2\pi)=e^{i\Theta 2\pi}\psi(\gamma) , \tag{1.12}$$

where $0\le\Theta\le1$. A specific value of Θ, or a specific gauge term, can be selected only on the basis of additional physical information about the system under consideration, as illustrated above.[8]

The electronic screening of the nuclear charges (1.10) can be interpreted also as due to the appearance of an additional vector potential distinct from the $e(\mathbf{H}_0\times\mathbf{R})/2c$ term, describing the interaction of the protons with the external magnetic field $\mathbf{H}_0$ in the symmetric gauge.[9] The concept of the geometric phase that emerges from this point of view, brought forward originally by Berry,[10] is of fundamental importance in classical and quantum mechanics.

It has been shown[11] that the presence of the gauge-coupling term in (1.9) results in the splitting of otherwise degenerate pairs of energy levels belonging to the two-dimensional representations of C_3. It turns out that when this splitting is of the right magnitude it can be rendered observable through its influence on the time evolution of the proton Zeeman polarization in the rotating frame. In order to eliminate the unwanted (and not completely understood) effect of lattice vibrations on methyl-group tunneling, the observations must be performed at low temperatures and in a time interval which is shorter than the nuclear spin-lattice relaxation time in the rotating frame. Furthermore, in a magnetic field of 1 T, the anticipated splitting of the degenerate E levels spans 30 kHz to 3 MHz, for a torsional tunneling frequency between 0.5 and 50 GHz. In this case the only transitions having any bearing on the time evolution of the magnetization in the rotating frame are those between the magnetic-flux-split E levels, driven solely by the intergroup dipole-dipole interactions.

The molecular system to be investigated by proton magnetization evolution is constrained by the following requirements.

(i) The tunneling frequency (A to E splitting) or frequencies (since in general an ensemble of interacting methyl groups is studied) must be in the GHz range.

(ii) The intergroup dipole-dipole interaction must be sufficiently strong; i.e., the CH_3 groups must be closely packed, for the spectral lines corresponding to the weak E to E transitions to be discernible above the noise level.

(iii) The coupling of the rotational motion of the methyl groups with the lattice vibrations must be weak; i.e., the temperature must be low, so that the concept of tunneling in the sense of quantum coherence[12] is applicable.

(iv) To properly understand the experimental results showing the effect of the gauge term, one should have at least an approximate picture of the energy-level scheme of interacting methyl groups under study.

As already indicated, the calculation to be compared with experiment is the Fourier transform of the time evolution of the proton Zeeman magnetization in the (spin) rotating frame. It is well known that in the limit of strong 90° pulses and at exact resonance the Fourier transform of the magnetization evolution in the rotating frame has a nonvanishing intensity only for transitions corresponding to the change of the magnetic quantum number $\Delta M=\pm2$. If, however, the strength of the 90° rf

pulse is comparable to the strength of the spin-locking field pulse, the evolution of the spins during the 90° pulse has to be taken into account as well. This evolution brings about an imaginary component in the Fourier transform at $\Delta M=\pm 1$.

In what follows we will analyze an ensemble of coupled pairs of methyl groups and calculate the Fourier transform of the proton magnetization evolution in powder samples and in a fictitious planar crystal, for a few special orientations of the methyl pair with respect to the external field. In addition, two inter-methyl-group distances will be considered, the near pairs corresponding to strongly and the more separated pairs to weakly coupled groups.

The calculated polycrystalline spectrum is then compared to the experimental spectra of proton magnetization evolution of methyl groups in acetyl acetone and dimethyltin dichloride. The calculated spectrum agrees qualitatively with the acetyl acetone spectrum if the charge on each proton is taken to be $0.1e$.

II. HAMILTONIAN AND THE EQUATION OF MOTION FOR THE DENSITY MATRIX

The Hamiltonian of the system describing the evolution of the proton magnetization during time intervals short compared to the spin-lattice relaxation time is

$$H=H_Z+H_R+H_D+H_{\rm rf}(t) . \tag{2.1}$$

The Zeeman Hamiltonian H_Z is given by

$$H_Z=-i\hbar\omega_0 I_z , \tag{2.2}$$

where ω_0 is the proton Zeeman frequency; $I_z\equiv\sum_{n=1}^{N}I_z^{(n)}$, with $I_z^{(n)}=I_{1z}^{(n)}+I_{2z}^{(n)}+I_{3z}^{(n)}$ being the z component of the total proton spin of the nth methyl group in a system consisting of N methyl groups. The rotational Hamiltonian H_R corresponding to (1.9) and generalized to a system of N interacting methyl groups is written as

$$H_R=\sum_{n=1}^{N}\left\{\frac{\hbar^2}{2I}\left[\frac{1}{i}\frac{\partial}{\partial\gamma_n}-\frac{3q}{hc}\Phi_n\right]^2+V_{3n}\left[1-\cos3(\gamma_n-\delta_n)\right]\right\}+\sum_{n<m}V(\gamma_n,\gamma_m) , \tag{2.3}$$

where q represents the effective proton charge defined in (1.10).

The magnetic flux Φ_n is defined by (1.3) and is

$$\frac{3e}{2\pi c}\Phi_n=\boldsymbol{\varepsilon}_3^{(n)}\cdot I\boldsymbol{\Omega} ,$$

where $\boldsymbol{\varepsilon}_3^{(n)}$ is the unit vector parallel to the symmetry axis of the nth methyl group. The Euler angles $(\alpha_n,\beta_n,\gamma_n)$ determine the orientation of the nth methyl group with respect to the laboratory coordinate system (xyz) with the z axis parallel to the external magnetic field $\mathbf{H}_0$.

The methyl-methyl interaction is included in (2.3) because in those cases where the transitions between the E levels are significant, this term is also likely to be important.

The dipole-dipole interaction is given by

$$H_D=\hbar\omega_D\sum_{k=-2}^{2}(-1)^k\sum_{i<j}U_{ij}^{-k}V_{ij}^{k} , \tag{2.4}$$

where $\omega_D=\gamma_p^2\hbar/R_0^3$. Here γ_p is the proton magnetogyric factor and $R_0\doteq 1.78$ Å is the proton-proton distance within a methyl group ($\omega_D\doteq 134$ kHz or $\omega_D/\gamma_p\doteq 5$ G). The operators U_{ij}^{-k} and V_{ij}^{k} are

$$U_{ij}^{-k}=(6\pi/5)^{1/2}\left[\frac{R_0}{R_{ij}}\right]^3 Y_2^{-k}(\theta_{ij},\phi_{ij}) , \tag{2.5}$$

where R_{ij} includes inter- as well as intra-methyl-group proton-proton distances. The spherical harmonics $Y_2^m(\theta_{ij},\phi_{ij})$ are defined according to the convention used in Ref. 13. (θ_{ij},ϕ_{ij}) are the polar angles of the proton-proton vector $\mathbf{R}_{ij}$ in the laboratory coordinate system (xyz). The spin operators V_{ij}^{k} are

$$V_{ij}^{0}=-(\tfrac{8}{3})^{1/2}[I_i^0I_j^0-\tfrac{1}{4}(I_i^+I_j^-+I_i^-I_j^+)] , \tag{2.6a}$$

$$V_{ij}^{\pm}=\pm(I_i^0I_j^{\pm}+I_i^{\pm}I_j^0) , \tag{2.6b}$$

$$V_{ij}^{\pm 2}=-I_i^{\pm}I_j^{\pm} , \tag{2.6c}$$

where we have introduced $I_i^0=I_{iz}$ and $I_i^{\pm}\equiv I_{ix}\pm iI_{iy}$. To simplify the notation we drop the superscript n because (2.4) contains both the intragroup and the intergroup dipole-dipole interactions.

The radio frequency field applied to the sample is the usual rotating transverse magnetic field. The interaction of the proton spins with this field is

$$H_{\rm rf}(t)=-\hbar\omega_1[I_x\cos\omega t-I_y\sin\omega t] , \tag{2.7}$$

where $\omega_1\equiv\gamma_pH_1$ and $I_x\equiv\sum_{n=1}^{N}I_x^{(n)}$ and the same for I_y. In (2.7) the rf field is considered to be a classical external field with a given time dependence and magnitude H_1.

The equation of motion for the density matrix ρ_r in the rotating frame at exact resonance $\omega=\omega_0$ is

$$i\hbar\frac{\partial\rho_r}{\partial t}=\left[-\hbar\omega_1I_x+H_R+e^{-i\omega_0tI_z}H_De^{i\omega_0tI_z},\rho_r\right] , \tag{2.8}$$

where ρ_r is related to the density matrix ρ in the laboratory frame by

$$\rho(t)=e^{i\omega_0tI_z}\rho_r(t)e^{-i\omega_0tI_z} . \tag{2.9}$$

It is easy to verify that

$$e^{-i\omega_0tI_z}H_De^{i\omega_0tI_z}=\hbar\omega_D\sum_{k=-2}^{2}(-1)^ke^{-ik\omega_0t}\sum_{i<j}U_{ij}^{-k}V_{ij}^{k} , \tag{2.10}$$

and since $\omega_1/\omega_0\doteq 10^{-3}$, we can drop the rapidly oscillating $k\neq 0$ terms in (2.8) to get

$$i\hbar\frac{\partial\rho_r}{\partial t}=\left[-\hbar\omega_1I_x+H_R+\hbar\omega_D\sum_{i<j}U_{ij}^0V_{ij}^0,\rho_r\right] . \tag{2.11}$$

To make the analogy with the laboratory frame stronger,

we make a second transformation, defined by

$$\sigma = e^{i(\pi/2)I_y} \rho_r e^{-i(\pi/2)I_y} , \tag{2.12}$$

resulting in

$$i\hbar \frac{\partial \sigma}{\partial t} = [H_0 + V, \sigma] , \tag{2.13}$$

where the notation

$$H_0 \equiv -\hbar\omega_1 I_z + H_R - \tfrac{1}{2}\hbar\omega_D \sum_{i<j} U_{ij}^0 V_{ij}^0 \tag{2.14}$$

and

$$\begin{aligned} V &\equiv (\tfrac{3}{8})^{1/2} \hbar\omega_D \sum_{i<j} U_{ij}^0 (V_{ij}^2 + V_{ij}^{-2}) \\ &\equiv (\tfrac{3}{8})^{1/2} (V^2 + V^{-2}) \end{aligned} \tag{2.15}$$

is introduced.

III. DETERMINATION OF THE LOWEST-ENERGY LEVELS OF H_0

We rewrite (2.14) as

$$H_0 = H_Z + H_R - \tfrac{1}{2} H_D^0 , \tag{3.1}$$

where $H_D^0 \equiv \hbar\omega_D \sum_{i<j} U_{ij}^0 V_{ij}^0$. Since $[H_Z, H_R] = [H_Z, H_D^0] = 0$, we can obtain the approximate solutions to the eigenvalue problem

$$H_0 \Psi = E \Psi \tag{3.2}$$

as products $\phi\chi$, where ϕ and χ are the eigenfunctions of H_R and H_Z, respectively. We have

$$H_R \phi(\gamma_1, \ldots, \gamma_N) = E^{(R)} \phi(\gamma_1, \ldots, \gamma_N) , \tag{3.3}$$

with H_R given by (2.3). According to (1.11), the ϕ's satisfy the periodic boundary conditions, with respect to all γ's. The symmetry group of H_R is assumed to be a direct product $C_3(1) \times C_3(2) \times \cdots \times C_3(N)$, so that the corresponding eigenfunctions are classified according to the irreducible representations of this group. As a consequence, they obey

$$\phi\left[\gamma_1 + p_1 \frac{2\pi}{3}, \ldots, \gamma_N + p_N \frac{2\pi}{3}\right] = \prod_{n=1}^{N} e^{i p_n s_n 2\pi/3} \phi(\gamma_1, \ldots, \gamma_N) , \tag{3.4}$$

where $p_n = 0$ or 1, $s_n = 0$, 1, or -1, if $\phi(\gamma_1, \ldots, \gamma_n, \ldots, \gamma_N)$ transforms with γ_n according to the A, E_a, or E_b irreducible representation, respectively, of the point group C_3. To solve (3.3) with H_R given by (2.3), we introduce

$$\phi(\gamma_1, \ldots, \gamma_N) = \left[\prod_{n=1}^{N} e^{(i3q/hc)\Phi_n \gamma_n}\right] \phi'(\gamma_1, \ldots, \gamma_N) . \tag{3.5}$$

The Schrödinger equation for ϕ' reads

$$\left\{\sum_{n=1}^{N} \left[-\frac{\hbar^2}{2I}\frac{\partial^2}{\partial\gamma_n^2} + V_{3n}[1 - \cos 3(\gamma_n - \delta_n)]\right] + \sum_{n<m} V(\gamma_n, \gamma_m)\right\} \phi' = E^{(R)} \phi' , \tag{3.6}$$

with the boundary conditions

$$\phi'(\gamma_1 + p_1 2\pi, \ldots, \gamma_N + p_N 2\pi) = \prod_{n=1}^{N} e^{-i(3q/hc)\Phi_n p_n 2\pi} \phi'(\gamma_1, \ldots, \gamma_N) . \tag{3.7}$$

Combining (3.7) with (3.4), we obtain

$$\phi'\left[\gamma_1 + p_1 \frac{2\pi}{3}, \ldots, \gamma_N + p_N \frac{2\pi}{3}\right] = e^{i\mathbf{k}\cdot\mathbf{l}} \phi'(\gamma_1, \ldots, \gamma_N) , \tag{3.8}$$

where we have defined the "wave vector" $\mathbf{k} \equiv (k_1, \ldots, k_N)$ with $k_n = -(3q\Phi_n/hc - s_n)$ and the "lattice vector" $\mathbf{l} \equiv (p_1(2\pi/3), \ldots, p_N(2\pi/3))$. Since condition (3.8) is recognized as the Bloch condition of solid-state physics, we anticipate the solutions of (3.6) to be Bloch sums as if one were dealing with a particle in a periodic lattice potential.

In what follows we shall restrict ourselves to a pair of coupled methyl groups. Let us denote by $U(\gamma_1, \gamma_2)$ the potential term in (2.3) describing a pair of groups only. We shall further assume that the solution $\gamma_c = (\gamma_{c1}, \gamma_{c2})$ of the equation

$$\frac{\partial U}{\partial \gamma_i} = 0, \quad i = 1, 2 , \tag{3.9}$$

exists and is such that the real symmetric matrix $\partial^2 U / \partial\gamma_{ci} \partial\gamma_{cj}$ is positive definite. Neglecting tunneling for the moment, we can construct a WKB ground-state wave function $\phi_0(\gamma_1 - \gamma_{c1}, \gamma_2 - \gamma_{c2})$ centered at the minimum γ_c of the potential $U(\gamma_1, \gamma_2)$ and satisfying the Schrödinger equation (3.6) with energy eigenvalue E_0. We normalize ϕ_0 on the rectangle $\gamma_{ci} - \pi/3 \le \gamma_i \le \gamma_{ci} + \pi/3$ for $i = 1, 2$. It follows that we can write $\phi'(\gamma_1, \gamma_2)$ in the zeroth-order approximation as

$$\phi'_{\nu_1\nu_2}(\gamma_1, \gamma_2) = C \sum_{n_1, n_2 = -\infty}^{\infty} e^{ik_1 n_1 2\pi/3} e^{ik_2 n_2 2\pi/3} \phi_0\left[\gamma_1 - \left(\gamma_{c1} + \frac{2\pi}{3} n_2\right), \gamma_2 - \left(\gamma_{c2} + \frac{2\pi}{3} n_2\right)\right] , \tag{3.10}$$

where $\nu_1, \nu_2 \in A$, E_a, or E_b, and C is a normalization constant. Inserting (3.10) into (3.6), we obtain[14]

$$E^{(R)}_{\nu_1\nu_2} \doteq E^{(R)}_{AA} + \frac{2}{3}\hbar\omega_{t1}\left\{\left[1 - \cos\left[\frac{2\pi}{3} s_1\right]\right] - \frac{q\Phi_1}{\hbar c}\sin\frac{2\pi}{3} s_1\right\} + \frac{2}{3}\hbar\omega_{t2}\left\{\left[1 - \cos\left[\frac{2\pi}{3} s_2\right]\right] - \frac{q\Phi_2}{\hbar c}\sin\frac{2\pi}{3} s_2\right\} , \tag{3.11}$$

where $\hbar\omega_{t1}=3(\hbar^2/2I)|a|$ and $\hbar\omega_{t2}=3(\hbar^2/2I)|b|$. The quantities a and b are given by

$$a=\int_{-\pi/3}^{\pi/3}d\gamma_2\left[\phi_0\left[-\frac{\pi}{3},\gamma_2\right]\frac{\partial\phi_0}{\partial\gamma_1}\left[\frac{\pi}{3},\gamma_2\right]-\phi_0\left[\frac{\pi}{3},\gamma_2\right]\frac{\partial\phi_0}{\partial\gamma_1}\left[-\frac{\pi}{3},\gamma_2\right]\right], \quad (3.12)$$

$$b=\int_{-\pi/3}^{\pi/3}d\gamma_1\left[\phi_0\left[\gamma_1,-\frac{\pi}{3}\right]\frac{\partial\phi_0}{\partial\gamma_2}\left[\gamma_1,\frac{\pi}{3}\right]-\phi_0\left[\gamma_1,\frac{\pi}{3}\right]\frac{\partial\phi_0}{\partial\gamma_2}\left[\gamma_1,\frac{\pi}{3}\right]\right]. \quad (3.13)$$

The energy-level scheme based on Eq. (3.11) together with the Zeeman energies, but excluding the dipolar shifts due to H_D^0, is shown in Fig. 1.

The above method of calculation is accurate if the overlap between pocket states localized in neighboring minima of the potential $U(\gamma_1,\gamma_2)$ is not too large, though it should be pointed out that no constraint was imposed on the magnitude of the interaction $V(\gamma_1,\gamma_2)$. Inclusion of overlaps between the next-nearest-neighboring minima reveals, for example, that levels, such as $E_{E_aE_b}$ and $E_{E_aE_a}$, are split. The magnitude of this splitting, however, is small compared to $\hbar\omega_{t1}$ and $\hbar\omega_{t2}$ and will not be considered further.

If there exist several distinct solutions $\gamma_c^{(i)}\equiv(\gamma_{c1}^{(i)},\gamma_{c2}^{(i)})$, not related by symmetry operations of the C_3 group, we must form a Bloch sum for each such solution separately, so that the general solution of (3.6) is then written as a linear combination of all Bloch sums. The situation is similar to the application of the linear combination of atomic orbitals (LCAO) method when we have more than one atom per unit cell.

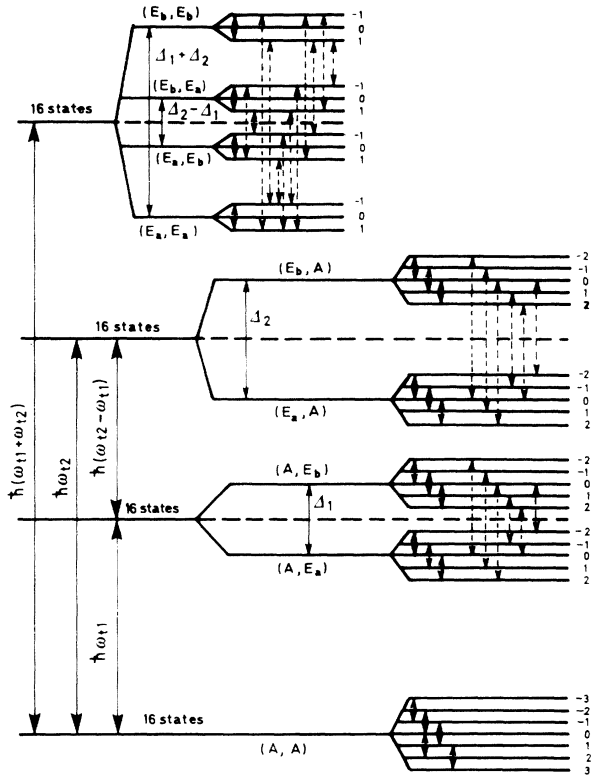

FIG. 1. Energy-level scheme corresponding to a pair of interacting methyl groups with arbitrary orientation. Only the lowest 64 states are shown. A, E_a, and E_b label the irreducible representations of the point group C_3. Solid and dashed lines indicate transitions induced by V.

The wave function $\phi_{\nu_1\nu_2}(\gamma_1,\gamma_2)$ follows from (3.5) and (3.10):

$$\phi_{\nu_1\nu_2}(\gamma_1,\gamma_2)=\left[\frac{1}{\sqrt{3}}\right]^2\sum_{n_1,n_2=-\infty}^{\infty}e^{i(2\pi/3)(n_1s_1+n_2s_2)}e^{i(3q/hc)\Phi_1[(\gamma_1-\gamma_{c1})-(2\pi/3)n_1]}e^{i(3q/hc)\Phi_2[(\gamma_2-\gamma_{c2})-(2\pi/3)n_2]}\times\phi_0\left[(\gamma-\gamma_{c1})-\frac{2\pi}{3}n_1,(\gamma-\gamma_{c2})-\frac{2\pi}{3}n_2\right], \quad (3.14)$$

with normalization defined on the square $\gamma_{ci}-\pi\le\gamma_i\le\gamma_{ci}+\pi$, $i=1,2$. [The unimportant phase factor $e^{i(3q/hc)(\Phi_1\gamma_{c1}+\Phi_2\gamma_{c2})}$ has been left out in (3.14).]

The wave function $\phi_{\nu_1\nu_2}(\gamma_1,\gamma_2)$ as given by (3.14) is defined on the interval $\gamma_i-\gamma_{ci}\in[-\pi,\pi]$ and is periodic with a period of 2π with respect to both variables γ_i. In the case of small overlap between neighboring minima, we may approximate it, for the purpose of calculating the matrix elements of H_D, with

$$\phi_{\nu_1\nu_2}(\gamma_1,\gamma_2)=\left[\frac{1}{\sqrt{3}}\right]^2\sum_{n_1,n_2=-1}^{1}e^{i(2\pi/3)(n_1s_1+n_2s_2)}\phi_0\left[\gamma_1-\frac{2\pi}{3}n_1,\gamma_2-\frac{2\pi}{3}n_2\right], \quad (3.15)$$

where $\gamma_1-\gamma_{ci}$ is replaced by γ_i and the phase factors containing the flux terms are omitted. This is permitted because $3e\Phi/hc\doteq0.24\times10^{-4}$ at most (when $H_0=1$ T). If the coupling term $V(\gamma_1,\gamma_2)$ in (2.3) is also dropped, then

$$\phi_0(\gamma_1,\gamma_2)=\phi_0(\gamma_1)\phi_0(\gamma_2),$$

which implies

$$\phi_{\nu_1\nu_2}(\gamma_1,\gamma_2)=\phi_{\nu_1}(\gamma_1)\phi_{\nu_2}(\gamma_2), \quad (3.16)$$

where $\phi_\nu(\gamma)$ is defined as

$$\phi_\nu(\gamma)=\frac{1}{\sqrt{3}}\left[\phi_0(\gamma)+e^{-i(2\pi/3)s}\phi_0\left[\gamma+\frac{2\pi}{3}\right]+e^{+i(2\pi/3)s}\phi_0\left[\gamma-\frac{2\pi}{3}\right]\right], \tag{3.17}$$

and $s=0$, 1, and -1 correspond to $\nu=A$, E_a, and E_b, respectively.

The eigenfunctions of the Zeeman Hamiltonian defined by the first term of (2.14), associated with the rotational vectors $\phi_{\nu_1\nu_2}$, are solutions of

$$H_Z\chi_{\tilde{\nu}_1}(I_1,M_1)\chi_{\tilde{\nu}_2}(I_2,M_2)=-(M_1+M_2)\hbar\omega_1\chi_{\tilde{\nu}_1}(I_1,M_1)\chi_{\tilde{\nu}_2}(I_2,M_2)\ , \tag{3.18}$$

where $\tilde{\nu}$ labels the irreducible representation of the point group C_3. The tilde over the subscript ν indicates conjugation so as to account for the restrictions imposed on the proton wave functions by the Pauli exclusion principle; i.e., if, for example, $\nu=E_a$, then $\tilde{\nu}=E_b$. The spin components $\chi_\nu(I,M)$ (I takes the values $\frac{3}{2}$ and $\frac{1}{2}$ and $-I\le M\le I$) are given explicitly as

$$\chi_A(\tfrac{3}{2},M)=\begin{cases}|+++\rangle,\\ \frac{1}{\sqrt{3}}[|++-\rangle+|+-+\rangle+|-++\rangle],\\ \frac{1}{\sqrt{3}}[|--+\rangle+|-+-\rangle+|+--\rangle],\\ |---\rangle\ ,\end{cases} \tag{3.19a}$$

and

$$\chi_{E_a}(\tfrac{1}{2},M)=\begin{cases}\frac{1}{\sqrt{3}}[|++-\rangle+\varepsilon|+-+\rangle+\varepsilon^*|-++\rangle],\\ \frac{1}{\sqrt{3}}[|--+\rangle+\varepsilon|-+-\rangle+\varepsilon^*|+--\rangle]\ ,\end{cases} \tag{3.19b}$$

where $\varepsilon\equiv e^{i2\pi/3}$ and $\chi_{E_b}(\frac{1}{2},M)=\chi^*_{E_a}(\frac{1}{2},M)$ (the asterisk denotes a complex-conjugate quantity).

To determine the energy eigenvalues of (3.1), we will neglect the mixing of degenerate levels caused by the inter-CH_3-dipole-dipole interaction. If the CH_3 groups are sufficiently far apart, this becomes an excellent approximation because of the factor $(R_0/R)^3$ in the dipole Hamiltonian. Here $R_0\doteq 1.78$ Å and R is the distance between the protons belonging to different methyl groups. This approximation is not essential in principle; however, it does simplify the calculations and enables us to obtain analytical expressions for the energy eigenvalues.

If, on the other hand, the methyl groups are close, some of the proton pairs may have R's even smaller than R_0, in which case the intergroup contribution to H_D^0 should not be neglected. This requires, at most, a solution of an 8×8 secular determinant, which, however, cannot be factored. In what follows, we will neglect the intergroup part of H_D^0 even if this may not be entirely justified for all the lattices studied.

Furthermore, to ensure that the splitting of E levels due to the magnetic field can be observed at all, we have to require $(E_{AE}^{(R)}-E_{AA}^{(R)})/\hbar$, $(E_{EA}^{(R)}-E_{AA}^{(R)})/\hbar$ to be of the order of 1 GHz or more. If the magnetic field is on the order of 1 T, then the splitting of E levels is approximately $\hbar\omega_D$ or larger. The magnitude of the rf field pulse used in the experiments was usually 15–40 G, implying that ω_1 is at least $3\omega_D$. Thus, if

$$E_{AE}^{(R)}-E_{AA}^{(R)}\gg\hbar\omega_0\gg\hbar\omega_1>\hbar\omega_D$$

is satisfied and the approximations introduced above are employed, the Hamiltonian H_0 is diagonal in the above basis. Using the formulas given in Appendix A and denoting the eigenvalues (3.2) as

$$H_0\phi_{\nu_1\nu_2}(\gamma_1,\gamma_2)\chi_{\tilde{\nu}_1}(I_1,M_1)\chi_{\tilde{\nu}_2}(I_2,M_2)=E(\nu_1M_1;\nu_2M_2)\phi_{\nu_1\nu_2}(\gamma_1,\gamma_2)\chi_{\tilde{\nu}_1}(I_1,M_1)\chi_{\tilde{\nu}_2}(I_2,M_2)\ , \tag{3.20}$$

we obtain the result

$$E(\nu_1M_1,\nu_2M_2)=E_{\nu_1\nu_2}^{(R)}-(M_1+M_2)\hbar\omega_1-\tfrac{1}{2}\langle\nu_2M_2,\nu_1M_1|H_D^0(\text{intra})|\nu_1M_1;\nu_2M_2\rangle\ , \tag{3.21}$$

where

$$\phi_{\nu_1\nu_2}\chi_{\tilde{\nu}_1}(I_1,M_1)\chi_{\tilde{\nu}_2}(I_2,M_2)\equiv|\nu_1M_1,\nu_2M_2\rangle\ .$$

Employing the approximations introduced in Appendix A, we obtain

$$\langle\nu_2M_2,\nu_1M_1|H_D^0(\text{intra})|\nu_1M_1,\nu_2M_2\rangle=-\tfrac{3}{8}\hbar\omega_D(1-3\cos^2\beta_1)\delta_{\nu_1,A}(\delta_{3/2,|M_1|}-\delta_{1/2,|M_1|})-\tfrac{3}{8}\hbar\omega_D(1-3\cos^2\beta_2)\delta_{\nu_2,A}(\delta_{3/2,|M_2|}-\delta_{1/2,|M_2|})\ . \tag{3.22}$$

δ_{ij} is the Kronecker delta and β_i is the angle between the symmetry axis of the ith methyl group and the direction of the external magnetic field.

IV. TIME EVOLUTION OF ZEEMAN POLARIZATION IN THE ROTATING FRAME

The equation of motion (2.13) for the density matrix σ in the rotating frame is solved by making a transformation to the interaction picture in the rotating frame defined by

$$\sigma_I(t)=e^{(i/\hbar)H_0 t}\sigma(t)e^{-(i/\hbar)H_0 t} . \tag{4.1}$$

Introducing

$$V(t)\equiv e^{(i/\hbar)H_0 t}Ve^{(-i/\hbar)H_0 t}=\exp\left\{\frac{i}{\hbar}\left[H_R-\frac{1}{2}H_D^0\right]t\right\}\left\{\frac{3}{8}\right\}^{1/2}\left[V^2e^{-i2\omega_1 t}+V^{-2}e^{+i2\omega_1 t}\right]\exp\left\{-\frac{i}{\hbar}\left[H_R-\frac{1}{2}H_D^0\right]t\right\} , \tag{4.2}$$

we can write $\sigma_I(t)$ as

$$\sigma_I(t)=\sum_{n=0}^{\infty}\sigma_I^{(n)}(t) , \tag{4.3}$$

where the successive approximations $\sigma_I^{(n)}(t)$ are

$$\sigma_I^{(n)}(t)=\left[-\frac{i}{\hbar}\right]^n\int_0^t dt_1\int_0^{t_1}dt_2\cdots\int_0^{t_{n-1}}dt_n[V(t_1),[V(t_2),[\cdots[V(t_n),\sigma_I(0)]\cdots] . \tag{4.4}$$

The density matrix at the beginning of the field pulse B (Fig. 2) is (see Appendix B)

$$\sigma_I(0)\cong\rho(0)+i\left[\frac{\beta_L\hbar\omega_0}{Z}\right]\frac{1}{\hbar\omega_1'}\int_0^{\pi/2}d\Theta\, e^{-i\mathcal{H}_R(\pi/2-\theta)}\sum_{k=-2}^{2}kd_{0k}(\theta)V^k e^{\mathcal{H}_R(\pi/2-\theta)} , \tag{4.5}$$

where $\rho(0)$ is the initial density matrix immediately prior to the application of a 90° pulse to the system in thermal equilibrium, i.e.,

$$\rho(0)=\frac{1}{Z}e^{-\beta_L(H_Z+H_R+H_D)}\doteq\frac{1}{Z}e^{-\beta_L(H_Z+H_R+H_D^0)} . \tag{4.6}$$

Here Z is the partition sum, $\beta_L\equiv 1/k_B T_L$, k_B is the Boltzmann constant, and T_L is the lattice temperature. The remaining symbols are defined in Appendix B.

The time evolution of Zeeman polarization in the rotating frame is observed as the expectation value of I_x in the laboratory frame after the end of the field pulse. In terms of the magnetization along the x direction, we have

$$M_x(t)=\gamma_p\hbar\langle I_x(t)\rangle=\gamma_p\hbar\,\mathrm{Tr}\{\rho(t)I_x\} , \tag{4.7}$$

where $\rho(t)$ is the density matrix in the laboratory frame (2.9). Using the expression for $\sigma_I(t)$, we can write

$$\langle I_x(t)\rangle=\mathrm{Tr}\{\sigma_I(t)I_z\}\cos\omega_0 t+\mathrm{Tr}\left\{\sigma_I(t)e^{(i/\hbar)H_0 t}I_y e^{-(i/\hbar)H_0 t}\right\}\sin\omega_0 t . \tag{4.8}$$

Taking Eqs. (4.2) and (4.4) and noting that

$$e^{(i/\hbar)H_0 t}I_y e^{-(i/\hbar)H_0 t}=\exp\left\{\frac{i}{\hbar}\left[H_R-\frac{1}{2}H_D^0\right]t\right\}(I_y\cos\omega_1 t-I_x\sin\omega_1 t)\exp\left\{-\frac{i}{\hbar}\left[H_R-\frac{1}{2}H_D^0\right]t\right\} , \tag{4.9}$$

we conclude that the coefficient of $\cos\omega_0 t$ in (4.8) will contain only multiples of $2\omega_1$, while the term proportional to $\sin\omega_0 t$ will include only odd multiples of ω_1, to all orders of the perturbation calculation. Using the basis defined by (3.20) as well as (4.4), (4.5), and (4.8), we obtain to second order in ω_D the result given in Appendix C, which confirms the above predictions. In higher orders we would obtain also $3\omega_1$, $4\omega_1$, etc. It is clear that the presence of terms with odd multiples of ω_1 is a consequence of partial dephasing of the spins during the 90° pulse.

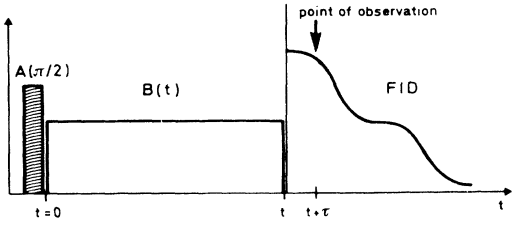

FIG. 2. Pulse sequence used in the experiments. $A(\pi/2)$ is the 90° pulse, while $B(t)$ is the spin-locking field pulse of variable duration.

V. EXPERIMENTAL DETAILS

All experiments were performed at a proton Larmor frequency of 30 MHz on a Bruker SXP variable frequency pulse spectrometer using a Waterloo NMR quadrature detector. The home-built probe assembly was used in conjunction with a Janis 5RD cryostat enabling pulse spin-locking experiments to be carried out to ~4 K. Temperature stability was maintained accurate to ±0.1 K using a home-built regulator with a carbon-glass sensor mounted in the sample area. A variety of materials was studied, chosen on the basis of inelastic neutron scattering (INS) $A \rightarrow E$ splitting assignments[15] to cover the range between ~0.1 and 15 GHz.

The samples were sealed under their own vapor pressure in 8-mm-o.d. thin-walled NMR tubes and cooled over a period of 1–2 h to 77 K. They were then exposed to ~1 Mrad of γ irradiation from a ^{60}Co source in order to introduce paramagnetic centers into the lattices, thereby reducing by orders of magnitude the T_1 (time needed for the saturated nuclear spins to reach equilibrium). Since Zeeman-tunneling transitions are not affected by the spin-lattice relaxation time T_1, this technique was invaluable in reducing experimentation time, thus minimizing errors introduced through temperature and rf matching variation, etc.

The experimental technique makes use of the spin-lock pulse sequence $A[\pi/2]_x B[H_1(t)]_y$ shown in Fig. 2. Pulse A "rotates" the equilibrium magnetization through 90° into the x-y plane where it is spin locked along the rf field (pulse B). The time evolution of the magnetization is obtained by measuring the amplitude of the signal immediately following spin locking as a function of the rf field pulse duration t. By increasing this time in unit increments Δt ($=1$ μs) for a total of N (~200) consecutive spin-locking steps (each delayed by $5T_1$ from its predecessor), one obtains a quasicontinuous oscillatory pattern which is then Fourier transformed to yield the spectrum.[16]

Data were acquired at 35 different "time windows" on the free induction decay (FID) using quadrature detection, whereby the absorption and dispersion components of the signal could be separately recorded and analyzed. Since the frequency profile of the spectra between time windows varied only in the random distribution of noise peaks, these could be averaged so as to optimize the signal to noise (S/N). Even with this optimization the S/N is only 10.

Although a number of systems with large $A \rightarrow E$ tunneling splittings were studied, only the spectra from polycrystalline acetyle-acetone and dimethyltin dichloride (shown in Figs. 7 and 8) have features which are indicative of a magnetic-flux effect. These two spectra are also representative of materials with strong and weak pairwise methyl-methyl coupling.

VI. DISCUSSION AND CONCLUSION

Equation (C1) shows that the time evolution of the magnetization in the rotating frame can in general be written as

$$M_x(t)-M_0\cos\omega_0 t=\sum_i p_i^{(1)}(\beta_1,\gamma_1)\{\sin[\omega_0-(\omega_1+\omega_i(\beta_1,\gamma_1))]t+\sin[\omega_0+(\omega_1+\omega_i(\beta_1,\gamma_1))]t\}$$
$$+\sum_j p_j^{(2)}(\beta_1,\gamma_1)\{-\sin[\omega_0-(2\omega_1+\omega_j(\beta_1,\gamma_1))]t+\sin[\omega_0+(2\omega_1+\omega_j(\beta_1,\gamma_1))]t\}$$
$$+\sum_k p_k^{(3)}(\beta_1,\gamma_1)\{\cos[\omega_0-(2\omega_1+\omega_k(\beta_1,\gamma_1))]t+\cos[\omega_0+(2\omega_k(\beta_1,\gamma_1))]t\}\ . \tag{6.1}$$

The Fourier transform of (6.1) is defined as

$$M_x(\omega)=\frac{1}{\sqrt{2\pi}}\int_{-\infty}^{\infty} dt\, M_x(t)e^{i\omega t}\ , \tag{6.2}$$

and the Gaussian broadening is introduced by

$$M_x(\omega,\sigma)=\int_{-\infty}^{\infty} du\, M_x(u)\frac{e^{-(\omega-u)^2/2\sigma^2}}{\sqrt{2\pi\sigma^2}}\ . \tag{6.3}$$

Choosing $\alpha_{12}=\beta_{12}=\gamma_{12}=\beta_1=0$ and the results obtained in Appendixes A and C, we calculated $M_x(\omega,\sigma)$ corresponding to the energy-level scheme shown in Fig. 4 (which is just a simplified version of the energy-level scheme shown in Fig. 1). We considered two different values of the intergroup distance characterized by the vector **a** as defined in Appendix C. We chose $\mathbf{a}=(2d,0,0)$ and $(1.75d,0,0)$ referred to in the future as the weak- and strong-coupling cases, respectively. $d=1.78$ Å is the intragroup proton-proton distance. Instead of using the frequency scale, we have introduced the off-field parameter $h=(\omega-\omega_0)/\gamma_p$. The remaining parameters used in the graphs are $\sigma=1$ G, $H_1=20$ G, $H_1'=40$ G, and $H_D\equiv\omega_D/\gamma_p=5$ G, while Δ, defined by (C2a) and illustrated in Fig. 4, corresponds to 15 and 22 G. It follows from the definition (6.2) and the expression

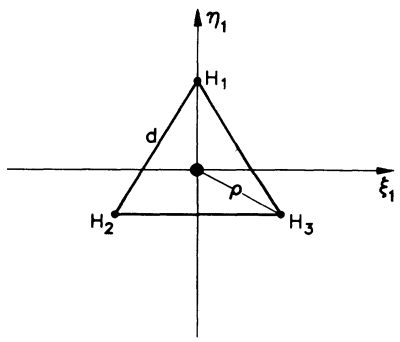

FIG. 3. Geometrical characteristics of a CH_3 group with respect to the methyl fixed-coordinate system.

(6.1) that $M_x(\omega)$ has a real component corresponding to the cosine terms and the imaginary component corresponding to the sine terms in (6.1). The real component is shown in Fig. 5 for the two values of the intergroup vector a denoted as the weak- and strong-coupling cases. In the limit $\Delta \rightarrow 0$, which is not shown, the real part of $M_x(\omega)$ shows appreciable intensity only in the vicinity of $h \cong 2H_1$, with a pronounced double peak characteristic of isolated methyl groups with tunneling frequency large compared to the strength of the intragroup dipole-dipole interaction. The splitting of the two dominant peaks in Fig. 5 is in agreement with this observation and is roughly equal to 5 G. On the other hand, the effect of the intergroup dipole-dipole interaction is seen in two ways. We note in Fig. 5, the strong-coupling case, the appearance of an additional line centered exactly at $h = 2H_1$. It is due to the transitions between the E levels, driven by the intergroup dipolar interaction (it is known that the E levels are not shifted by the intragroup dipolar interaction). The second more interesting effect of the intergroup dipolar interaction, and which is the object of our analysis, is the occurrence of the satellites on the low-field side of the double peak. The position of the satellites and their intensities are determined by the magnitude of the magnetic-flux splitting Δ and by the strength of the intergroup dipolar interaction, respectively. As seen from Fig. 5, the intensity of the satellites is approximately 40% of the intensity of the dominant double peak in the strong-coupling case.

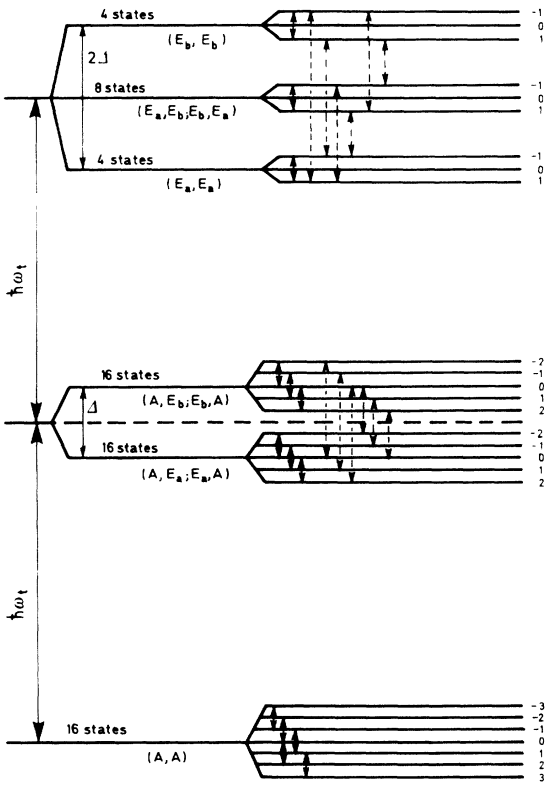

FIG. 4. Energy-level scheme of a pair of noninteracting methyl groups, coupled only by their intergroup dipole-dipole interactions with $\cos\beta_1 = \cos\beta_2$.

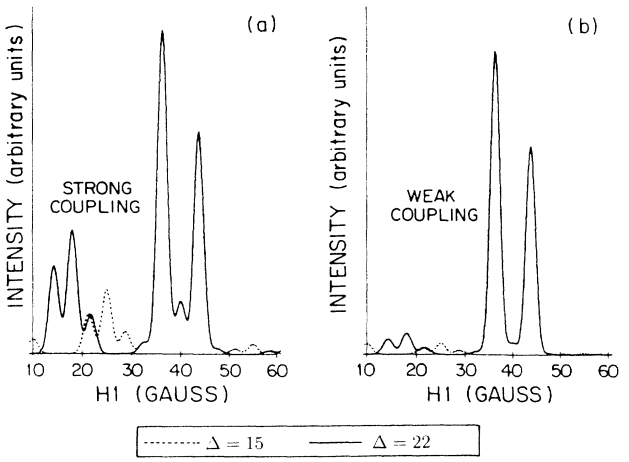

FIG. 5. Calculated spectra for the case of a fictitious crystal where all methyl C_3 axes are aligned parallel to the external field $\mathbf{H}_0$. (a) and (b) show the expected line shapes for strong and weak pairwise coupling between adjacent methyl groups. Transitions among the magnetic-flux-split E states are clearly visible in (a). The solid and dotted curves correspond to a magnetic-flux splitting of $\Delta = 22$ and 15 G, respectively.

Contrary to the real component of $M_x(\omega)$, the imaginary part shows a nonvanishing intensity, proportional to $1/H_1'$, both at H_1 and $2H_1$. When H_1' and the intensity of the spin-locking field pulse H_1 are of comparable magnitude, the intensity of the imaginary component at $h \cong 2H_1$ is about the same as the intensity of the real component. On the other hand, the relative intensity of the imaginary component around $h \cong H_1$ turns out to be at least one order of magnitude larger than its intensity at $h \cong 2H_1$, when $H_1' = 40$ G and $H_1 = 20$ G. The satellites generated by the intergroup-dipolar-driven transitions between the magnetically split E levels are visible also in the imaginary component of the Fourier spectrum, $M_x(\omega)$. However, the satellites centered in the range $H_1 \leq h \leq 2H_1$ are usually distorted or even hidden because of overlapping of intragroup dipolar components of the Fourier spectrum. Also, the satellites on the low-field side of the strong double peak at $h \cong H_1$ are not very useful because the experimental spectra in this range of h values are not very reliable. It is therefore our conclusion that the real part of $M_x(\omega)$ is much more appropriate for the analysis of Δ satellites.

So far, we have been discussing $M_x(\omega)$ for a crystal, i.e., for fixed values of β_1 and γ_1. To obtain the results for powder samples, we introduce the powder average of the Zeeman polarization by

$$\langle M_x(t) \rangle = \frac{1}{4\pi} \int_0^{2\pi} d\gamma_1 \int_{-1}^{1} d\cos\beta_1 M_x(t) . \tag{6.4}$$

Its Fourier transform $\langle M_x(\omega) \rangle$ and the broadened version $\langle M_x(\omega,\sigma) \rangle$ are again defined according to (6.2) and (6.3), respectively. Using the definition of the δ function

$$\delta(x) = \frac{1}{2\pi} \int_{-\infty}^{\infty} dt\, e^{ixt}$$

and its property

$$\delta[g(x)]=\sum_j \delta(x-x_j)\Big/\left|\frac{dg(x_j)}{dx_j}\right| ,$$

where x_j are the simple zeros of $g(x_j)=0$ ($dg(x_j)/dx_j\neq 0$), we obtain, considering (6.1), a typical term of $\langle M_x(\omega)\rangle$ in the form

$$\sum_j \frac{1}{4\pi}\int_0^{2\pi} d\gamma_1 \frac{p(\beta_1^{(j)},\gamma_1)}{|\partial\omega(\beta_1^{(j)},\gamma_1)/\partial\cos\beta_1^{(j)}|} , \tag{6.5}$$

where $\cos\beta_1^{(j)}$ are solutions of

$$\Omega=n\omega_1+\omega(\beta_1,\gamma_1),\quad n=1,2 , \tag{6.6}$$

and $\Omega\cong\gamma_p h$. $\omega(\beta_1,\gamma_1)$ and $p(\beta_1,\gamma_1)$ are defined by (C1), (C8), (C9), and (6.1).

To calculate the Fourier transform $\langle M_x(\omega)\rangle$ for an arbitrary relative orientation of the interacting pair is tedious and will not be done here. However, to illustrate the general result (6.1), we shall consider the special case $\alpha_{12}=\beta_{12}=\gamma_{12}=0$. It follows from (C8) that $\omega_D(\beta_2)=\omega_D(\beta_1)$, and all the frequencies ω_i, ω_j, and ω_k entering (6.1) depend on $\cos\beta_1$ only. In this case (6.5) simplifies to

$$\sum_j \frac{1}{2}\left|\frac{d\omega(\cos\beta_1^{(j)})}{d(\cos\beta_1^{(j)})}\right|^{-1}\frac{1}{2\pi}\int_0^{2\pi} d\gamma_1 p(\beta_1^{(j)},\gamma_1) . \tag{6.7}$$

As can be seen from (C1), in this particular case the γ_1 dependence enters only through $U^0_{\nu_1\nu_2}$. Using (C7), we obtain

$$\begin{aligned}&\frac{1}{2\pi}\int_0^{2\pi} d\gamma_1 |U^0_{\nu_1\nu_2}(\beta_1,\gamma_1)|^2\\ &\quad=\tfrac{3}{32}a_{\nu_1\nu_2}(1-3\cos^2\beta_1)^2+\tfrac{27}{64}b_{\nu_1\nu_2}(1-\cos^2\beta_1)^2\\ &\qquad+\tfrac{27}{4}c_{\nu_1\nu_2}\cos^2\beta_1(1-\cos^2\beta_1) ,\end{aligned} \tag{6.8}$$

where the coefficients a, b, and c for the weak- and strong-coupling cases are given in Table I.

With the help of (6.7) and (6.8), we calculated $\langle M_x(h,\sigma)\rangle$ for $\alpha_{12}=\beta_{12}=\gamma_{12}=0$. The resulting imaginary and real components are shown in Fig. 6. The parameters used are $H_1=20$ G, $H_1'=40$ G, $H_D=5$ G, $\sigma=1$ G, and $\Delta/\gamma_p=15$ and 22 G. Graphs (c) and (d) in Fig. 6, representing the real part of $\langle M_x(h,\sigma)\rangle$, are qualitatively similar to the single-crystal spectra shown in Fig. 5. We note, however, that the satellite structure is spread out and its intensity is decreased. The ratio of the satellite intensity and the intensity of the peak centered at $2H_1$ is approximately 1:10 and as such difficult to observe. Moreover, comparing the graphs corresponding to weak and strong coupling we see that the characteristic double-peak structure has disappeared in the strong-coupling case due to the transitions within the E manifolds driven by the intergroup dipole-dipole interaction.

The imaginary component of $\langle M_x(h,\sigma)\rangle$ shown in Fig. 6(b) is not very interesting as far as satellites are concerned because of the large intensity of the peak centered at H_1. The ratio of the intensity of this peak to the intensity of the satellites is of the order of 100:1; therefore, the latter are not visible.

To conclude this section, we emphasize again that the magnetization as given by (C1) or (6.1) is evaluated immediately after the end of the field pulse H_1 (see Fig. 2). Experimentally, however, the measurement of the FID signal is delayed for a time τ (~ 6 μs or more) after the end of the field pulse. For this reason the evolution of the magnetization in the laboratory frame under the action of $-\hbar\omega_0 I_z+H_R+H_D$ has to be taken into account. A calculation entirely analogous to the one described previously yields

$$\begin{aligned}M_x(t+\tau)=&\gamma_p\hbar\,\mathrm{Tr}\left[e^{-i\omega_1 tI_z}\exp\left\{\frac{i}{\hbar}\left[H_R-\frac{1}{2}H_D^0\right](t+\tau)\right\}U(\tau)I_z U^\dagger(\tau)\right.\\ &\left.\times\exp\left\{\frac{i}{\hbar}\left[H_R-\frac{1}{2}H_D^0\right](t+\tau)\right\}e^{i\omega_1 tI_z}\sigma_I(t)\right]\cos\omega_0(t+\tau)\\ &+\gamma_p\hbar\,\mathrm{Tr}\left[e^{-i\omega_1 tI_z}\exp\left\{\frac{i}{\hbar}\left[H_R-\frac{1}{2}H_D^0\right](t+\tau)\right\}U(\tau)I_y U^\dagger(\tau)\right.\\ &\left.\times\exp\left\{\frac{i}{\hbar}\left[H_R-\frac{1}{2}H_D^0\right](t+\tau)\right\}e^{i\omega_1 tI_z}\sigma_I(t)\right]\sin\omega_0(t+\tau) ,\end{aligned} \tag{6.9}$$

where

$$U(\tau)=T\left\{\exp\left[\frac{i}{\hbar}\int_0^\tau ds\,\bar{V}(s)\right]\right\} , \tag{6.10}$$

with T representing the time ordering operator and

$$\begin{aligned}\bar{V}(s)=&\exp\left\{-\frac{i}{\hbar}\left[H_R-\frac{1}{2}H_D^0\right]s\right\}V\\ &\times\exp\left\{\frac{i}{\hbar}\left[H_R-\frac{1}{2}H_D^0\right]s\right\} .\end{aligned} \tag{6.11}$$

In the limit $H_1'\to\infty$, the term proportional to

TABLE I. Coefficients $a_{\nu_1\nu_2}$, $b_{\nu_1\nu_2}$, and $c_{\nu_1\nu_2}$ as defined by Eq. (6.8). The upper part of the table corresponds to $\mathbf{a}=(2d,0,0)$ and the bottom part to $\mathbf{a}=(1.75d,0,0)$, $d=1.78$ Å.

	AA	AE_a	E_aA	E_aE_a	E_aE_b
a	3.6/9	1.1/9	1.1/9	0.6/9	0.5/9
b	2.9/9	1/9	1/9	1/9	0.6/9
c	0	0	0	0	0
a	14.1/9	6.2/9	6.2/9	4.3/9	3.7/9
b	13/9	6.0/9	6.0/9	5.3/9	4.4/9
c	0	0	0	0	0

$\sin\omega_0(t+\tau)$ in (6.9) goes to zero and we will consider only the first term proportional to $\cos\omega_0(t+\tau)$ which generates the real part of $M_x(\omega,\sigma)$ (the Fourier transform is performed with respect to t). In the lowest order, $U(\tau)$ is replaced by 1 and we obtain the τ-independent spectrum discussed earlier. In the next higher order, we have to consider

$$U^{(1)}(\tau)I_z+I_zU^{(1)\dagger}(\tau)\ ,$$

where

$$U^{(1)}(\tau)=\frac{1}{\hbar}\int_0^\tau ds\ \bar{V}(s)\ .$$

This term will yield a τ-dependent contribution to the real part of $M_x(\omega,\sigma)$ with frequencies centered at $2H_1$, including the satellites, and the intensity of some of the lines could be comparable to the τ-independent part of the spectrum. When we go to the second order, as far as the $U(\tau)$ evolution is concerned, we encounter terms such as

$$U^{(2)}(\tau)I_z+I_zU^{(2)\dagger}(\tau)+U^{(1)}(\tau)I_zU^{(1)\dagger}(\tau)\ ,$$

where

$$U^{(2)}(\tau)=\left[\frac{i}{\hbar}\right]^2\int_0^\tau d\tau_1\int_0^{\tau_1}d\tau_2\bar{V}(\tau_1)\bar{V}(\tau_2)\ .$$

Here again we obtain the τ-dependent contribution to the real part of the Fourier transform, but of lower intensity than the τ-independent part. In addition, we also obtain a Fourier component centered at Δ/γ_p; however, its intensity is down by a factor $[H_D(\text{inter})/\hbar\Delta]^2$ compared to the intensity of the τ-independent Δ satellites. All in all, the evolution in the high field does change the detailed structure of the spectrum, especially when Δ becomes comparable to ω_D, but it has no bearing whatsoever on the position of the peaks. The most interesting aspect of the τ evolution is the emergence of the line centered at Δ/γ_p, which may become observable for Δ's of the order of ω_D.

It has been shown that the magnetic splitting of E levels is proportional to the effective charge q whose magnitude is determined by nonadiabatic screening of proton charges by the methyl-group electrons. This screening can be interpreted also as another example of the geometrical phase effects in molecular systems, the universality of which has been recognized especially since the work of Berry.[10] In our calculation we have demonstrated that the optimal conditions to study this effect are obtained in monocrystals where the satellites resulting from the split-

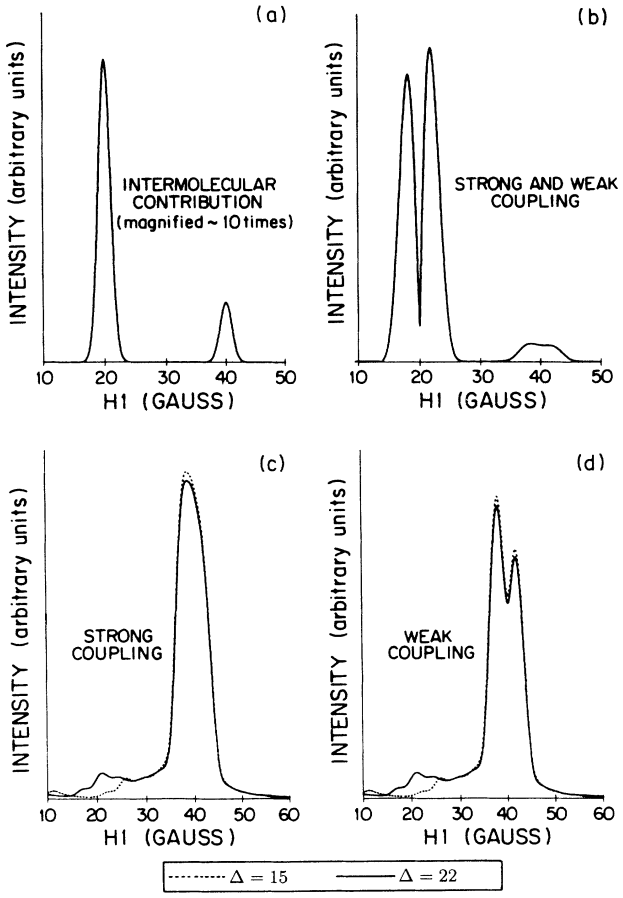

FIG. 6. Calculated spectra for a polycrystalline (powder) sample. (a) The small intermolecular contribution occurring at H_1 and $2H_1$, magnified times 10 relative to the other figures. (b) Dispersion (imaginary) component of the powder averaged transform for both the strong- and weak-coupling cases, showing a split H_1 peak and a low-intensity peak at $2H_1$. (c) and (d) Absorption (real) spectrum for strongly and weakly pairwise coupled methyl groups, respectively. The small feature in the vicinity of 20 G in both figures is due to transitions among the magnetic-flux-split E states. The solid and dotted curves correspond to a magnetic-flux splitting of 22 and 15 G, respectively.

ting of the E levels are well pronounced (Fig. 5). This is unfortunately no longer true for a polycrystalline powder sample where the spectral features of interest are only about 10% of the main $2\omega_1$ peak intensity (Fig. 6). It should be kept in mind that the oscillatory part of the proton magnetization represents only 5–20% of the measured signal M_0, thus making good signal to noise crucial. Furthermore, the characteristic "A-E" splitting has to be in the GHz range in order to produce the magnetic splitting of the E levels comparable to the intensity of the spin-locking field pulse H_1, whose optimal value was found to be 15–25 G.

Of the 21 materials studied, 9 have A-E splittings between 5 and 12 GHz. Only two, shown in Figs. 7 and 8, show features which could be attributed to the magnetic flux. The proton spectrum of acetyl acetone in particular has a small satellite, the center of which is 38 kHz below the $2\omega_1$ peak. This satellite shift agrees with the calculation in which the proton charge is set at 0.1e.

In summary, we have presented a set of calculations yielding the expected spectra of a system of pairwise coupled tunneling methyl groups, driving nonsecular dipolar transitions among the magnetic-flux-split E states. These are visible as small, low-frequency satellites of the $\Delta M=2$ dipolar peak in the spectrum of the magnetization evolution in the rotating frame. Furthermore, the shape of the calculated $\Delta M=2$ dipolar peak itself, which

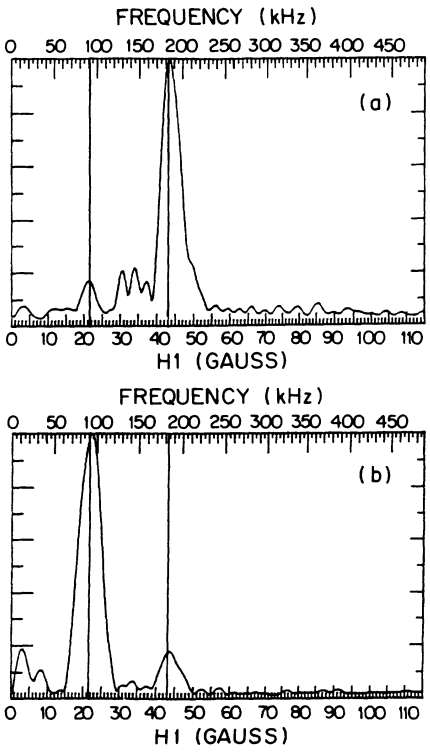

FIG. 7. Experimental spectrum of 2, 4 pentanedione (acetyl acetone) at 10 K and a Larmor frequency of 30 MHz illustrating the strong pairwise coupling case. The reported $A-E$ tunneling splitting is 10 GHz. (a) Absorption and (b) dispersion spectra showing the positions of (from left to right) H_1 and $2H_1$ as full-scale vertical lines.

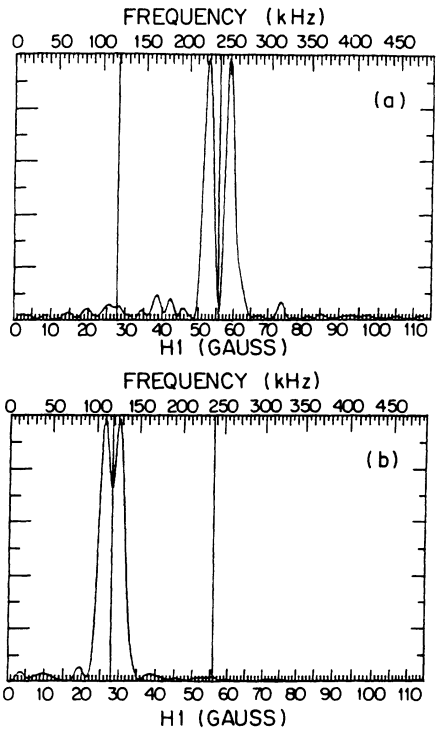

FIG. 8. Experimental spectrum of dimethyltin dichloride at 10 K and 30 MHz corresponding to weak pairwise intermethyl coupling. The reported $A-E$ tunneling splitting is 11.8 GHz. (a) Absorption and (b) dispersion spectra.

does not depend strongly on the relative orientation of the neighboring groups, is in good agreement with experiment for both weakly and strongly coupled methyl groups as shown by the spectra of acetyl acetone and dimethyltin dichloride (Figs. 7 and 8, respectively). This agreement supports our calculations conclusively.

ACKNOWLEDGMENTS

Support from the National Science and Engineering Research Council, Ottawa is gratefully acknowledged.

APPENDIX A

The matrix elements of the dipole-dipole interaction, in the basis spanned by the eigenfunctions of H_R+H_Z and denoted by $\phi_{\nu_1\nu_2}\times\chi_{\tilde{\nu}_1}\chi_{\tilde{\nu}_2}$, are calculated most conveniently if H_D is written in the symmetry-adapted form. Let us write H_D defined by (2.4) as a sum of an intragroup and an intergroup operator,

$$H_D=H_D(\text{intra})+H_D(\text{inter})\ . \tag{A1}$$

The symmetry-adapted forms are

$$H_D(\text{intra})=\hbar\omega_D\sum_{k=-2}^{2}(-1)^k[U_A^{-k}V_A^k+U_{E_a}^{-k}V_{E_b}^k+U_{E_b}^{-k}V_{E_a}^k]\ , \tag{A2}$$

where

$$\begin{bmatrix} X_A \\ X_{E_a} \\ X_{E_b} \end{bmatrix} = \frac{1}{\sqrt{3}} \begin{bmatrix} 1 & 1 & 1 \\ 1 & \varepsilon^* & \varepsilon \\ 1 & \varepsilon & \varepsilon^* \end{bmatrix} \begin{bmatrix} X_{12} \\ X_{23} \\ X_{31} \end{bmatrix} , \tag{A3}$$

and X_{ij} stands for U_{ij}^{-k} or V_{ij}^{k}; and

$$H_D(\text{inter}) = \hbar\omega_D \sum_{k=-2}^{2} (-1)^k \sum_{\nu_1,\nu_2} U_{\nu_1\nu_2}^{-k} V_{\bar{\nu}_1\bar{\nu}_2}^{k} , \tag{A4}$$

with $\nu_i \in A, E_a, E_b$ and

$$\chi_{\nu_1\nu_2} = \sum_{i=1}^{3}\sum_{j=1}^{3} S_{\nu_1 i} S_{\nu_2 j} X_{ij} . \tag{A5}$$

The matrix S is defined in (A3).

If we take X_{ij} to be U_{ij}, we obtain

$$\begin{bmatrix} U^0_{AA} \\ U^0_{AE_a} \\ U^0_{AE_b} \\ U^0_{E_aA} \\ U^0_{E_aE_a} \\ U^0_{E_aE_b} \\ U^0_{E_bA} \\ U^0_{E_bE_a} \\ U^0_{E_bE_b} \end{bmatrix} = \frac{1}{3} \begin{bmatrix} 1 & 1 & 1 & 1 & 1 & 1 & 1 & 1 & 1 \\ 1 & \varepsilon^* & \varepsilon & 1 & \varepsilon^* & \varepsilon & 1 & \varepsilon^* & \varepsilon \\ 1 & \varepsilon & \varepsilon^* & 1 & \varepsilon & \varepsilon^* & 1 & \varepsilon & \varepsilon^* \\ 1 & 1 & 1 & \varepsilon^* & \varepsilon^* & \varepsilon^* & \varepsilon & \varepsilon & \varepsilon \\ 1 & \varepsilon^* & \varepsilon & \varepsilon^* & \varepsilon & 1 & \varepsilon & 1 & \varepsilon^* \\ 1 & \varepsilon & \varepsilon^* & \varepsilon^* & 1 & \varepsilon & \varepsilon & \varepsilon^* & 1 \\ 1 & 1 & 1 & \varepsilon & \varepsilon & \varepsilon & \varepsilon^* & \varepsilon^* & \varepsilon^* \\ 1 & \varepsilon^* & \varepsilon & \varepsilon & 1 & \varepsilon^* & \varepsilon^* & \varepsilon & 1 \\ 1 & \varepsilon & \varepsilon^* & \varepsilon & \varepsilon^* & 1 & \varepsilon^* & 1 & \varepsilon \end{bmatrix} \begin{bmatrix} U^0_{11} \\ U^0_{12} \\ U^0_{13} \\ U^0_{21} \\ U^0_{22} \\ U^0_{23} \\ U^0_{31} \\ U^0_{32} \\ U^0_{33} \end{bmatrix} .$$

In the actual calculations of the dipole-dipole matrix elements, we shall always make the approximation

$$\int_{-\pi}^{\pi}\int_{-\pi}^{\pi} d\gamma_1 d\gamma_2 \phi^*_{\nu_1\nu_2}(\gamma_1,\gamma_2)\phi_{\nu_1'\nu_2'}(\gamma_1,\gamma_2)\langle \chi_{\bar{\nu}_1}(I_1M_1)\chi_{\bar{\nu}_2}(I_2M_2)|H_D|\chi_{\bar{\nu}_1'}(I_1'M_1')\chi_{\bar{\nu}_2'}(I_2'M_2')\rangle$$

$$\doteq \frac{1}{9}\sum_{n_1,n_2} e^{i(2\pi/3)[n_1(s_1'-s_1)+n_2(s_2'-s_2)]} \int_{-\pi}^{\pi}\int_{-\pi}^{\pi} d\gamma_1 d\gamma_2 \left|\phi_0\left(\gamma_1-\frac{2\pi}{3}n_1,\gamma_2-\frac{2\pi}{3}n_2\right)\right|^2$$

$$\times \langle \chi_{\bar{\nu}_1}(I_1M_1)\chi_{\bar{\nu}_2}(I_2M_2)|H_D|\chi_{\bar{\nu}_1'}(I_1'M_1')\chi_{\bar{\nu}_2'}(I_2'M_2')\rangle , \tag{A6}$$

and assume moreover that $\phi_0(\gamma_1,\gamma_2)$ is so sharply peaked around the minimum of the potential $U(\gamma_1,\gamma_2)$ that the matrix element in (A6) can be taken out of the integral.

APPENDIX B

The pulse sequence applied to the sample in thermal equilibrium at temperature T_L in the external magnetic field is shown in Fig. 2. Consequently, in order to determine the initial value of the density matrix $\sigma_I(0)$, the evolution of the spin system due to the 90° pulse has also to be considered. The rf field corresponding to the 90° pulse is along the negative y axis, with the corresponding interaction Hamiltonian given by analogy with (2.7) as

$$H'_{\text{rf}}(t) = +\hbar\omega_1'[I_x \sin\omega_0 t + I_y \cos\omega_0 t] . \tag{B1}$$

Repeating the calculation outlined in Sec. II, we obtain

$$i\hbar\frac{\partial\rho_r}{\partial t} = [\hbar\omega_1' I_y + H_R + H_D^0, \rho_r] , \tag{B2}$$

where $\rho_r(0)=\rho(0)$ and is given by (4.6), and $\omega_1' \equiv \gamma_p H_1'$ (H_1' is the intensity of the 90° pulse). Equation (B2) has a formal solution

$$\rho_r(\theta) = U(\theta)\rho_r(0)U^+(\theta) , \tag{B3}$$

where

$$U(\theta) = e^{-i(I_y + \mathcal{H}_R + \mathcal{H}_D^0)\theta} , \tag{B4}$$

$\theta \equiv \omega_1' t$, $\mathcal{H}_R \equiv H_R/\hbar\omega_1'$, and $\mathcal{H}_D^0 \equiv H_D^0/\hbar\omega_1'$. We can write $U(\theta)$ in a form convenient for later applications as

$$U(\theta) = e^{-i(I_y+\mathcal{H}_R)\theta}[1 - iU'(\theta)] , \tag{B5}$$

where

$$U'(\theta) = \int_0^\theta d\theta_1 \mathcal{H}_D^0(\theta_1) - i\int_0^\theta d\theta_1 \int_0^{\theta_1} d\theta_2 \mathcal{H}_D^0(\theta_1)\mathcal{H}_D^0(\theta_2) + \cdots \tag{B6}$$

and

$$\mathcal{H}_D^0(\theta) = e^{i\mathcal{H}_R\theta} \sum_k d_{0k}(\theta) V^k e^{-i\mathcal{H}_R\theta}/\hbar\omega_1' . \tag{B7}$$

Here

$$V^k = \hbar\omega_D \sum_{i<j} U_{ij}^0 V_{ij}^k ,$$

and the matrix coefficients $d_{0k}(\theta)$ are given as[17]

$$d_{00}(\theta) = (3\cos^2\theta - 1)/2 ,$$

$$d_{0\pm1}(\theta) = \pm(\tfrac{3}{2})^{1/2}\sin\theta\cos\theta ,$$

$$d_{0\pm2}(\theta) = (\tfrac{3}{8})^{1/2}\sin^2\theta .$$

Using the transformation (2.12), we obtain

$$\sigma(\theta)=e^{-i\mathcal{H}_R\theta}\{\sigma_0(\theta)+i[\sigma_0(\theta)U''^{+}(\theta)-U''(\theta)\sigma_0(\theta)]+U''(\theta)\sigma_0(\theta)U''^{+}(\theta)\}e^{i\mathcal{H}_R\theta}\ , \tag{B8}$$

where

$$\sigma_0(\theta)=\frac{1}{Z}\exp\left\{-\beta_L\left[-\hbar\omega_0(I_z\sin\theta-I_x\cos\theta)+H_R+\hbar\omega_D\sum_k d_{0k}(\pi/2-\theta)V^k\right]\right\} \tag{B9}$$

and

$$U''(\theta)=e^{i(\pi/2-\theta)I_y}U'(\theta)e^{-i(\pi/2-\theta)I_y}\ . \tag{B10}$$

In the case of an ideal 90° pulse perfectly uniform across the whole sample and a valid high-temperature approximation, we obtain, for $\theta=\pi/2$,

$$\sigma(\pi/2)\equiv\sigma_I(t=0)\cong\rho(0)+\frac{i\beta_L\hbar\omega_0}{Z}\frac{1}{\hbar\omega_1'}\int_0^{\pi/2}d\theta\, e^{-i\mathcal{H}_R(\pi/2-\theta)}\sum_k kd_{0k}(\theta)V^k e^{i\mathcal{H}_R(\pi/2-\theta)}\ , \tag{B11}$$

where $\rho(0)$ is given by the high-temperature approximation of Eq. (4.6). The result (B11) thus represents the initial density matrix describing the spin-rotational system at the moment when the spin-locking field pulse $B(H_1)$ is switched on.

APPENDIX C

Here we give the explicit expression for $M_x(t)$ as defined by (4.7). To obtain this result, we had to calculate a number of matrix elements of the dipolar Hamiltonian. We have done this by using the symmetry-adapted expressions for the dipolar interactions given in Appendix A; the approximations described briefly at the end of Appendix A were also used:

$$\begin{aligned}
&\frac{[M_0\cos\omega_0 t-M_x(t)]/\gamma_p\hbar}{4\beta_L\hbar\omega_0/Z}\\
&=\left[\frac{9}{2}\left[\frac{\omega_D}{\omega_1'}\right]\sum_{i=1}^{2}(1-3\cos^2\beta_i)\left[\cos\left[\omega_1+\frac{3}{4}\omega_D(\beta_i)\right]t-\cos\left[\omega_1-\frac{3}{4}\omega_D(\beta_i)\right]t\right]\right.\\
&\quad+\frac{27}{16}\sum_{i=1}^{2}(1-3\cos^2\beta_i)^2\left\{\frac{\omega_D^2}{\omega_1'[2\omega_1+\frac{3}{4}\omega_D(\beta_i)]}\left[\cos\omega_1 t-\cos\left[\omega_1+\frac{3}{4}\omega_D(\beta_i)\right]t\right]\right.\\
&\qquad\left.\left.+\frac{\omega_D^2}{\omega_1'(2\omega_1-\frac{3}{4}\omega_D(\beta_i)}\left[\cos\omega_1 t-\cos\left[\omega_1-\frac{3}{4}\omega_D(\beta_i)\right]t\right]\right\}\right.\\
&\quad+2|U^0_{AE_a}|^2\left[\frac{2}{3}[f_1(\delta_{EE}-\Delta_2\cos\beta_2;t)+f_1(\delta_{EE}+\Delta_2\cos\beta_2;t)]+f_2(\Delta_2\cos\beta_2,\omega_D(\beta_1);t)\right]\\
&\quad+2|U^0_{E_aA}|^2\left[\frac{2}{3}[f_1(\delta_{EE}-\Delta_1\cos\beta_1;t)+f_1(\delta_{EE}+\Delta_1\cos\beta_i;t)]+f_2(\Delta_1\cos\beta_1,\omega_D(\beta_2);t)\right]\\
&\quad+|U^0_{E_aE_a}|^2\left[\frac{16}{3}f_1(\Delta_1\cos\beta_1+\Delta_2\cos\beta_2;t)+f_3(\Delta\omega_R^{(3)},\omega_D(\beta_1),\omega_D(\beta_2);t)+f_3(\Delta\omega_R^{(4)},\omega_D(\beta_1),\omega_D(\beta_2);t)\right]\\
&\quad+|U^0_{E_aE_b}|^2\left[\frac{16}{3}f_1(\Delta_1\cos\beta_1-\Delta_2\cos\beta_2;t)+f_3(\Delta\omega_R^{(1)},\omega_D(\beta_1),\omega_D(\beta_2);t)+f_3(\Delta\omega_R^{(2)},\omega_D(\beta_1),\omega_D(\beta_2);t)\right]\Bigg]\sin\omega_0 t\\
&\quad+\left[\left[\frac{27}{16}(1-3\cos^2\beta_1)^2+\frac{5}{6}|U^0_{AA}|^2\right]g_1\left[\frac{3}{4}\omega_D(\beta_1);t\right]+\left[\frac{27}{16}(1-3\cos^2\beta_2)^2+\frac{5}{6}|U^0_{AA}|^2\right]g_1\left[\frac{3}{4}\omega_D(\beta_2);t\right]\right.\\
&\qquad+\frac{3}{4}|U^0_{AA}|^2\left[g_1\left[\frac{3}{4}\omega_D(\beta_1)+\frac{3}{4}\omega_D(\beta_2);t\right]+g_1\left[\frac{3}{4}\omega_D(\beta_1)-\frac{3}{4}\omega_D(\beta_2);t\right]\right]\\
&\qquad+|U^0_{AA}|^2g_1(0;t)+\frac{\pi}{2}\left[\frac{27}{32}(1-\cos^2\beta_1)^2+\frac{5}{12}|U^0_{AA}|^2\right]g_2\left[\frac{3}{4}\omega_D(\beta_1);t\right]\\
&\qquad\left.+\frac{\pi}{2}\left[\frac{27}{32}(1-3\cos^2\beta_2)^2+\frac{5}{12}|U^0_{AA}|^2\right]g_2\left[\frac{3}{4}\omega_D(\beta_2);t\right]\right.
\end{aligned}$$

$$
\begin{aligned}
&+\frac{\pi}{2}\frac{3}{8}|U^0_{AA}|^2\left[g_2\left[\frac{3}{4}\omega_D(\beta_1)+\frac{3}{4}\omega_D(\beta_2);t\right]+g_2\left[\frac{3}{4}\omega_D(\beta_1)-\frac{3}{4}\omega_D(\beta_2);t\right]\right]+\frac{\pi}{2}\frac{1}{2}|U^0_{AA}|^2 g_2(0;t)\\
&+|U^0_{AE_a}|^2\left[g\left[\Delta_2\cos\beta_2,\Delta_2\cos\beta_2+\frac{3}{4}\omega_D(\beta_1);t\right]+g\left[\Delta_2\cos\beta_2,\Delta_2\cos\beta_2-\frac{3}{4}\omega_D(\beta_1);t\right]\right.\\
&\qquad+\frac{4}{3}g(\Delta_2\cos\beta_2,\Delta_2\cos\beta_2;t)\\
&\qquad\left.+\frac{1}{3}[g(\delta_{EE}+\Delta_2\cos\beta_2,\delta_{EE}+\Delta_2\cos\beta_2;t)+g(\delta_{EE}-\Delta_2\cos\beta_2,\delta_{EE}-\Delta_2\cos\beta_2;t)]\right]\\
&\qquad+|U^0_{E_aA}|^2\left[g\left[\Delta_1\cos\beta_1,\Delta_1\cos\beta_1+\frac{3}{4}\omega_D(\beta_2);t\right]+g\left[\Delta_1\cos\beta_1,\Delta_1\cos\beta_1-\frac{3}{4}\omega_D(\beta_2);t\right]\right.\\
&\qquad\qquad+\frac{4}{3}g(\Delta_1\cos\beta_1,\Delta_1\cos\beta_1;t)\\
&\qquad\qquad\left.+\frac{1}{3}[g(\delta_{EE}+\Delta_1\cos\beta_1,\delta_{EE}+\Delta_1\cos\beta_1;t)+g(\delta_{EE}-\Delta_1\cos\beta_1,\delta_{EE}-\Delta_1\cos\beta_1;t)]\right]\\
&+\frac{4}{3}|U^0_{E_aE_a}|^2 g(\Delta_1\cos\beta_1+\Delta_2\cos\beta_2,\Delta_1\cos\beta_1+\Delta_2\cos\beta_2;t)\\
&+\frac{4}{3}|U^0_{E_aE_b}|^2 g(\Delta_1\cos\beta_1-\Delta_2\cos\beta_2,\Delta_1\cos\beta_1-\Delta_2\cos\beta_2;t)\\
&+\left[|U^0_{E_aE_b}|^2\sum_{i=1}^{2}+|U^0_{E_aE_a}|^2\sum_{i=3}^{4}\right]\left\{\frac{1}{4}\left[g\left[\Delta\omega_R^{(i)},\Delta\omega_R^{(i)}+\frac{3}{8}\omega_D(\beta_1)+\frac{3}{8}\omega_D(\beta_2);t\right]\right.\right.\\
&\qquad\left.+g\left(\Delta\omega_R^{(i)},\Delta\omega_R^{(i)}-\frac{3}{8}\omega_D(\beta_1)-\frac{3}{8}\omega_D(\beta_2);t\right]\right.\\
&\left.\left.+\frac{1}{12}g\left[\Delta\omega_R^{(i)},\Delta\omega_R^{(i)}+\frac{3}{8}\omega_D(\beta_1)-\frac{3}{8}\omega_D(\beta_2);t\right]+\frac{3}{4}g\left[\Delta\omega_R^{(i)},\Delta\omega_R^{(i)}-\frac{3}{8}\omega_D(\beta_1)+\frac{3}{8}\omega_D(\beta_2);t\right]\right\}\right]\cos\omega_0 t\ . \qquad \text{(C1)}
\end{aligned}
$$

The notation used in (C1) is as follows:

$$\Delta_i=(\tfrac{4}{3})^{1/2}\omega_{ti}q\Phi_0/\hbar c\ , \qquad \text{(C2a)}$$

where $\Phi_0=\pi\rho^2H_0$ is the magnetic flux through the circle traced out by the protons of the methyl group. In particular, if we choose $H_0=1$ T and $q=e$, then $\Delta_i\doteq 0.6\times10^{-4}\omega_{ti}$. For $\omega_t=2$ GHz it follows that $\Delta\doteq 120$ kHz or $\Delta/\gamma_p\doteq 4.5$ G. It could be misleading that ω_t is given in frequency units, e.g., 2 GHz, yet it is the angular velocity $\omega_t=2\pi\nu_t$. It follows that $\nu_t=2/2\pi$ GHz. The $\hbar\delta_{EE}$ is the difference between the E_aE_a and E_aE_b levels in the absence of the external magnetic field as discussed briefly in Sec. III and is included for the sake of generality only; also, $M_0=\hbar\gamma_p\mathrm{Tr}[I_z\rho(0)]$:

$$\omega_D(\beta)=-\tfrac{1}{2}\omega_D(1-3\cos^2\beta)\ , \qquad \text{(C2b)}$$

$$\Delta\omega_R^{(1)}=(\omega_{t2}-\omega_{t1})+\tfrac{1}{2}(\Delta_2\cos\beta_2-\Delta_1\cos\beta_1)\ , \qquad \text{(C2c)}$$

$$\Delta\omega_R^{(2)}=(\omega_{t2}-\omega_{t1})-\tfrac{1}{2}(\Delta_2\cos\beta_2-\Delta_1\cos\beta_1)\ , \qquad \text{(C2d)}$$

$$\Delta\omega_R^{(3)}=(\omega_{t2}-\omega_{t1})+\tfrac{1}{2}(\Delta_2\cos\beta_2+\Delta_1\cos\beta_1)\ , \qquad \text{(C2e)}$$

$$\Delta\omega_R^{(4)}=(\omega_{t2}-\omega_{t1})-\tfrac{1}{2}(\Delta_2\cos\beta_2+\Delta_1\cos\beta_1)\ , \qquad \text{(C2f)}$$

and

$$g_1(x;t)=\frac{\omega_D^2[1-\cos(2\omega_1+x)t]}{(2\omega_1+x)^2}+\frac{\omega_D^2[1-\cos(2\omega_1-x)t]}{(2\omega_1-x)^2}\ , \qquad \text{(C3a)}$$

$$g_2(x;t)=\frac{\omega_D^2\sin(2\omega_1+x)t}{\omega_1'(2\omega_1+x)}+\frac{\omega_D^2\sin(2\omega_1-x)t}{\omega_1'(2\omega_1-x)}\ , \qquad \text{(C3b)}$$

$$g_3(x;t)=\frac{\omega_D^2[1-\cos(2\omega_1+x)t]}{\omega_1'(2\omega_1+x)}-\frac{\omega_D^2[1-\cos(2\omega_1-x)t]}{\omega_1'(2\omega_1-x)} \qquad \text{(C3c)}$$

$$g(x,y;t)=g_1(y;t)+\left[\frac{4\omega_1'^2[1-\cos(\pi x/2\omega_1')]-2x^2}{(x/\omega_1')(x^2-4\omega_1'^2)}\right]\frac{1}{2}g_3(y;t)-\frac{4\omega_1'^2}{x^2-4\omega_1'^2}\frac{\sin(\pi x/2\omega_1')}{(x/\omega_1')}\frac{1}{2}g_2(y;t)\ . \tag{C3d}$$

Finally, the f_i functions are

$$f_1(x;t)=\left[\frac{\omega_1'^2}{x^2-4\omega_1'^2}\right]\left[\frac{\omega_D^2}{4\omega_1^2-x^2}\right]\left\{\frac{(2\omega_1+x)}{\omega_1'}[\cos(\omega_1-x)t-\cos\omega_1 t]+\frac{2\omega_1-x}{\omega_1'}[\cos(\omega_1+x)t-\cos\omega_1 t]\right\}, \tag{C4a}$$

$$\begin{aligned}f_2(x,y;t)=&\left[\frac{\omega_1'^2}{x^2-4\omega_1'^2}\right]\left[\frac{\omega_D^2}{\omega_1'(2\omega_1+x+\frac{3}{4}y)}\left\{\left[\cos(\omega_1+x)t-\cos\left[\omega_1+\frac{3}{4}y\right]t\right]+\left[\cos\left[\omega_1+x+\frac{3}{4}y\right]t-\cos\omega_1 t\right]\right\}\right.\\&+\frac{\omega_D^2}{\omega_1'(2\omega_1-x-\frac{3}{4}y)}\left\{\left[\cos(\omega_1-x)t-\cos\left[\omega_1-\frac{3}{4}y\right]t\right]+\left[\cos\left[\omega_1-x-\frac{3}{4}y\right]-\cos\omega_1 t\right]\right\}\\&+\frac{8}{3}\left[\frac{\omega_D^2}{\omega_1'(2\omega_1+x)}[\cos(\omega_1+x)t-\cos\omega_1 t]+\frac{\omega_D^2}{\omega_1'(2\omega_1-x)}(\cos(\omega_1-x)t-\cos\omega_1 t)\right]\\&+\frac{\omega_D^2}{\omega_1'(2\omega_1+x-\frac{3}{4}y)}\left\{\left[\cos\left[\omega_1+x-\frac{3}{4}y\right]t-\cos\omega_1 t\right]+\left[\cos(\omega_1+x)t-\cos\left[\omega_1-\frac{3}{4}y\right]t\right]\right\}\\&\left.+\frac{\omega_D^2}{\omega_1'(2\omega_1-x+\frac{3}{4}y)}\left\{\left[\cos(\omega_1-x)t-\cos\left[\omega_1+\frac{3}{4}y\right]t\right]+\left[\cos\left[\omega_1-x+\frac{3}{4}y\right]t-\cos\omega_1 t\right]\right\}\right],\end{aligned} \tag{C4b}$$

$$\begin{aligned}f_3(x,y_1,y_2;t)=&\left[\frac{\omega_1'^2}{x^2-4\omega_1'^2}\right]\left[\frac{1}{2}\frac{\omega_D^2}{\omega_1'[2\omega_1+x-\frac{3}{8}(y_1+y_2)]}\right.\\&\times\left\{\left[\cos\left[\omega_1+x-\frac{3}{8}(y_1+y_2)\right]t-\cos\omega_1 t\right]\right.\\&\left.+\left[\cos\left[\omega_1+x-\frac{3}{8}(y_2-y_1)t\right]-\cos\left[\omega_1-\frac{3}{4}y_1\right]t\right]\right\}+\frac{1}{2}\frac{\omega_D^2}{\omega_1'[2\omega_1+x+\frac{3}{8}(y_1+y_2)]}\\&\times\left\{\left[\cos\left[\omega_1+x+\frac{3}{8}(y_1+y_2)\right]t-\cos\omega_1 t\right]\right.\\&\left.+\left[\cos\left[\omega_1+x-\frac{3}{8}(y_2-y_1)\right]t-\cos\left[\omega_1+\frac{3}{4}y_2\right]t\right]\right\}+\frac{1}{2}\frac{\omega_D^2}{\omega_1'[2\omega_1-x-\frac{3}{8}(y_1+y_2)]}\\&\times\left\{\left[\cos\left[\omega_1-x-\frac{3}{8}(y_1+y_2)\right]t-\cos\omega_1 t\right]\right.\\&\left.+\left[\cos\left[\omega_1-x+\frac{3}{8}(y_2-y_1)\right]t-\cos(\omega_1-\frac{3}{4}y_2)t\right]\right\}+\frac{1}{2}\frac{\omega_D^2}{\omega_1'[2\omega_1-x+\frac{3}{8}(y_1+y_2)]}\\&\times\left\{\left[\cos\left[\omega_1-x+\frac{3}{8}(y_1+y_2)\right]t-\cos\omega_1 t\right]\right.\\&\left.+\left[\cos\left[\omega_1-x+\frac{3}{8}(y_2-y_1)\right]t-\cos\left[\omega_1+\frac{3}{4}y_1\right]t\right]\right\}+\frac{3}{2}\frac{\omega_D^2}{\omega_1'[2\omega_1+x+\frac{3}{8}(y_2-y_1)]}\\&\times\left\{\left[\cos\left[\omega_1+x-\frac{3}{8}(y_1+y_2)\right]t-\cos\left[\omega_1+\frac{3}{4}y_2\right]t\right]\right.\end{aligned} \tag{C4c}$$

$$+\left[\cos\left[\omega_1+x+\frac{3}{8}(y_1+y_2)\right]t-\cos\left[\omega_1-\frac{3}{4}y_1\right]t\right]\Bigg\}+\frac{3}{2}\frac{\omega_D^2}{\omega_1'[2\omega_1-x-\frac{3}{8}(y_2-y_1)]}$$

$$\times\Bigg\{\left[\cos\left[\omega_1-x+\frac{3}{8}(y_1+y_2)\right]t-\cos\left[\omega_1-\frac{3}{4}y_2\right]t\right]$$

$$+\left[\cos\left[\omega_1-x-\frac{3}{8}(y_1+y_2)\right]t-\cos\left[\omega_1+\frac{3}{4}y_1\right]t\right]\Bigg\}$$

$$+\frac{1}{3}\frac{\omega_D^2}{\omega_1'[2\omega_1+x-\frac{3}{8}(y_2-y_1)]}\left[\cos\left[\omega_1+x-\frac{3}{8}(y_2-y_1)\right]t-\cos\omega_1 t\right]$$

$$+\frac{1}{3}\frac{\omega_D^2}{\omega_1'[2\omega_1-x+\frac{3}{8}(y_2-y_1)]}\left[\cos\left[\omega_1-x+\frac{3}{8}(y_2-y_1)\right]t-\cos\omega_1 t\right]\Bigg]. \tag{C4c}$$

The quantities $U^0_{\nu_1\nu_2}$ are defined in Appendix A and are, in general, functions of the Euler angles determining the relative orientation of the two interacting methyl groups and their orientation with respect to the external magnetic field $\mathbf{H}_0$. In order to obtain explicit formulas for $U^0_{\nu_1\nu_2}$ as functions of Euler angles, we choose the coordinate system (ξ_1,η_1,ζ_1) fixed in the methyl group (labeled 1) (Fig. 3). The proton-proton distance $d\doteq 1.78$ Å determines $\rho\doteq 1.03$ Å.

The coordinates of the three protons belonging to the methyl group 1, with respect to the coordinate system (ξ_1,η_1,ζ_1), are denoted as $(\xi_1^{(1)},\eta_1^{(1)},\zeta_1^{(1)})$ and are given in Table II. The second methyl group (labeled 2) is oriented in the same manner with respect to its own coordinate system (ξ_2,η_2,ζ_2). However, the coordinate system (ξ_2,η_2,ζ_2) is rotated with respect to the coordinate system (ξ_1,η_1,ζ_1) through Euler angles $(\alpha_{12},\beta_{12},\gamma_{12})$. The coordinates $(\xi_2^{(2)},\eta_2^{(2)},\zeta_2^{(2)})$ of the protons belonging to the second methyl group can be written, with the rotation matrix $D^{(1)}_{m',m}(\alpha_{12},\beta_{12},\gamma_{12})$, in terms of their components in system (ξ_1,η_1,ζ_1). We denote them as $(\xi_1^{(2)},\eta_1^{(2)},\zeta_1^{(2)})$, and are given in Table III. From now on all vectors will be written in coordinate system (ξ_1,η_1,ζ_1). The proton-proton vector $\mathbf{R}_{ij}$ pointing from the ith proton in the first methyl group to the jth proton of the second group is

$$\begin{aligned} R_{ij}\equiv&(\xi^{(12)}+\xi_i^{(2)}-\xi_j^{(1)}\,,\\ &\eta^{(12)}+\eta_1^{(2)}-\eta_j^{(1)}\,,\\ &\zeta^{(12)}+\zeta_i^{(2)}-\zeta_j^{(1)})\,, \end{aligned} \tag{C5}$$

where the vector $\mathbf{a}\equiv(\xi^{(12)},\eta^{(12)},\zeta^{(12)})$ points from the origin of the coordinate system (ξ_1,η_1,ζ_1) to the origin of the coordinate system (ξ_2,η_2,ζ_2). The components $\xi_i^{(2)},\xi_j^{(1)}$, etc., are given in Tables II and III. The spherical polar coordinates $(\theta'_{ij},\theta'_{ij})$, which determine the orientation of $\mathbf{R}_{ij}$ with respect to the coordinate system (ξ_1,η_1,ζ_1), are defined with

$$\cos\theta'_{ij}=\frac{(\xi^{(12)}+\xi_i^{(2)}-\xi_j^{(1)})}{R_{ij}}\,, \tag{C6a}$$

$$\tan\phi'_{ij}=\frac{(\eta^{(12)}+\eta_i^{(2)}-\eta_j^{(1)})}{(\xi^{(12)}+\xi_i^{(2)}-\xi_j^{(1)})}\,. \tag{C6b}$$

Now we can write U^0_{ij}, using the rotation matrices $D^{(2)}_{m',m}(\alpha_1\beta_1,\gamma_1)$, as

$$\begin{aligned} U^0_{ij}=&\left[\frac{3}{2}\right]^{1/2}\left[\frac{R_0}{R_{ij}}\right]^3\\ &\times\{\tfrac{1}{4}(3\cos^2\beta_1-1)(3\cos^2\theta'_{ij}-1)\\ &+\tfrac{3}{4}\sin^2\beta_1\sin^2\theta'_{ij}\cos2(\gamma_1+\phi'_{ij})\\ &-3\sin\beta_1\cos\beta_1\sin\theta'_{ij}\cos\theta'_{ij}\cos(\gamma_1+\phi'_{ij})\}\,, \end{aligned} \tag{C7}$$

where $R_0\equiv d=1.78$ Å. $U^0_{\nu_1\nu_2}$ can be obtained by using (A5) and (C7).

In the same manner we can express $\omega_D(\beta_2)$, defined by (C2b), in terms of $(\alpha_1,\beta_1,\gamma_1)$ and $(\alpha_{12},\beta_{12},\gamma_{12})$. The result is

$$\begin{aligned} \omega_D(\beta_2)=\omega_D\{&\tfrac{1}{4}(3\cos^2\beta_1-1)(3\cos^2\beta_{12}-1)\\ &+\tfrac{3}{4}\sin^2\beta_1\sin^2\beta_{12}\cos2(\gamma_1+\alpha_{12})\\ &-3\sin\beta_1\cos\beta_1\sin\beta_{12}\cos\beta_{12}\cos(\gamma_1+\alpha_{12})\}\,. \end{aligned} \tag{C8}$$

TABLE II. Proton coordinates with respect to the methyl-group fixed-coordinate system (ξ,η,ζ).

	$\xi_1^{(1)}$	$\eta_1^{(1)}$	$\zeta_1^{(1)}$
$H1$	0	$d\sqrt{3}/3$	0
$H2$	$-d/2$	$-d\sqrt{3}/6$	0
$H3$	$d/2$	$-d\sqrt{3}/6$	0

TABLE III. Proton coordinates of the second methyl group expressed in the coordinate system fixed with respect to the first methyl group. The Euler angles $(\alpha_{12},\beta_{12},\gamma_{12})$ determine the orientation of the second CH_3 group relative to the first one.

	$\xi_1^{(2)}$	$\eta_1^{(2)}$	$\zeta_1^{(2)}$
$H1$	$\frac{-d\sqrt{3}}{6}[(1+\cos\beta_{12})\sin(\alpha_{12}+\gamma_{12})+(1-\cos\beta_{12})\sin(\alpha_{12}-\gamma_{12})]$	$\frac{d\sqrt{3}}{6}[(1+\cos\beta_{12})\cos(\alpha_{12}+\gamma_{12})+(1-\cos\beta_{12})\cos(\alpha_{12}-\gamma_{12})]$	$\frac{d\sqrt{3}}{3}\sin\beta_{12}\sin\gamma_{12}$
$H2$	$\frac{d\sqrt{3}}{6}\left\{(1+\cos\beta_{12})\left[-\frac{\sqrt{3}}{2}\cos(\alpha_{12}+\gamma_{12})+\frac{1}{2}\sin(\alpha_{12}+\gamma_{12})\right]+(1-\cos\beta_{12})\times\left[\frac{\sqrt{3}}{2}\cos(\alpha_{12}-\gamma_{12})+\frac{1}{2}\sin(\alpha_{12}-\gamma_{12})\right]\right\}$	$\frac{d\sqrt{3}}{6}\left\{(1+\cos\beta_{12})\left[-\frac{\sqrt{3}}{2}\sin(\alpha_{12}+\gamma_{12})-\frac{1}{2}\cos(\alpha_{12}+\gamma_{12})\right]-(1-\cos\beta_{12})\times\left[-\frac{\sqrt{3}}{2}\sin(\alpha_{12}-\gamma_{12})+\frac{1}{2}\cos(\alpha_{12}-\gamma_{12})\right]\right\}$	$-\frac{d\sqrt{3}}{3}\sin\beta_{12}\left[-\frac{\sqrt{3}}{2}\cos\gamma_{12}+\frac{1}{2}\sin\gamma_{12}\right]$
$H3$	$\frac{d\sqrt{3}}{6}\left\{(1+\cos\beta_{12})\left[\frac{\sqrt{3}}{2}\cos(\alpha_{12}+\gamma_{12})+\frac{1}{2}\sin(\alpha_{12}+\gamma_{12})\right]+(1-\cos\beta_{12})\times\left[-\frac{\sqrt{3}}{2}\cos(\alpha_{12}-\gamma_{12})+\frac{1}{2}\sin(\alpha_{12}-\gamma_{12})\right]\right\}$	$\frac{d\sqrt{3}}{6}\left\{(1+\cos\beta_{12})\left[\frac{\sqrt{3}}{2}\sin(\alpha_{12}+\gamma_{12})-\frac{1}{2}\cos(\alpha_{12}+\gamma_{12})\right]-(1-\cos\beta_{12})\times\left[\frac{\sqrt{3}}{2}\sin(\alpha_{12}-\gamma_{12})+\frac{1}{2}\cos(\alpha_{12}-\gamma_{12})\right]\right\}$	$-\frac{d\sqrt{3}}{3}\sin\beta_{12}\left[\frac{\sqrt{3}}{2}\cos\gamma_{12}+\frac{1}{2}\sin\gamma_{12}\right]$

In particular,

$$\cos\beta_2=\cos\beta_1\cos\beta_{12}-\sin\beta_1\sin\beta_{12}\cos(\gamma_1+\alpha_{12})\ . \tag{C9}$$

In the case of a powder sample, the Euler angles $(\alpha_1\beta_1\gamma_1)$ cover the range $0\le\alpha_1\le2\pi$, $0\le\beta_1\le\pi$, and $0\le\gamma_1\le2\pi$, while $(\alpha_{12},\beta_{12},\gamma_{12})$ are fixed parameters which are determined by the crystallographic structure of the material studied.

[1]P. Schmelcher, L. S. Cederbaum, and H. D. Meyer, J. Phys. B **21**, L445 (1988); Phys. Rev. A **38**, 6066 (1988).

[2]J. Peternelj and T. Kranjc (unpublished).

[3]E. Merzbacher, Am. J. Phys. **30**, 237 (1962).

[4]P. Marmet and L. J. Binette, J. Phys. B **11**, 3707 (1978).

[5]I. N. Levine, *Quantum Mechanics and Electronic Structure*, Quantum Chemistry Vol. I (Allyn and Bacon, Boston, 1970).

[6]S. Clough, P. J. McDonald, and F. O. Zelaya, J. Phys. C **17**, 4413 (1984); S. Clough, G. J. Barker, K. J. Abed, and A. J. Horsewill, Phys. Rev. Lett. **60**, 136 (1988).

[7]M. Reed and B. Simon, *Methods of Modern Mathematical Physics* (Academic, New York, 1980), Vol. I.

[8]L. S. Schulman, J. Math. Phys. **12**, 304 (1971).

[9]W. N. Cottingham and N. Hassan, J. Phys. B **23**, 323 (1990); C. A. Mead, Rev. Mod. Phys. **64**, 51 (1992).

[10]M. V. Berry, Proc. R. Soc. London A **392**, 45 (1984).

[11]J. Peternelj, I. Jenčič, B. Cvikl, and M. M. Pintar, Phys. Rev. B **39**, 6374 (1989).

[12]A. J. Leggett, Prog. Theor. Phys. Suppl. **60**, 80 (1980).

[13]G. Arfken, *Mathematical Methods for Physicists*, third ed. (Academic, New York, 1985).

[14]J. Peternelj and I. Jenčič, J. Phys. A **22**, 1941 (1989).

[15]M. Prager and A. Heidemann, Tunneling Spectroscopy Compilation of Available Data, Institut Laue-Langevin, 156X, F-38042 Grenoble Cedex, France.

[16]D. W. Nicoll and M. M. Pintar, Phys. Rev. B **23**, 1064 (1981).

[17]P. S. Hubbard, Rev. Mod. Phys. **33**, 249 (1961).